

Interaction between the Tethyan and Paleo-Pacific tectonic domains in Southeast Asia: Late Triassic initiation of an inward-dipping double subduction system

Qi Zhao¹, Yi Yan^{1*}, Andrew Carter², Peter D. Clift^{3,4}, Jonny Wu⁵, Junaidi Bin Asis⁶, Zuofei Zhu⁷, Shihao Gou¹, Yang Zhou⁸

¹Guangzhou Institute of Geochemistry, Chinese Academy of Sciences, Guangzhou 510640, China

²School of Natural Sciences, Birkbeck, University of London, London, WC1E 7HX, UK

³Department of Earth Sciences, University College London, London WC1E 6BS, UK

⁴Institute of Marine and Environmental Sciences, University of Szczecin, Mickiewicza 16, 70-383 Szczecin, Poland

⁵Department of Geosciences, University of Arizona, Tucson, AZ, USA

⁶Faculty of Science and Natural Resources, Jalan UMS, 88400 Kota Kinabalu, Sabah, Malaysia

⁷Sanya Institute of South China Sea Geology, Guangzhou Marine Geological Survey, Sanya 572025, China

⁸School of National Safety and Emergency Management, Beijing Normal University, Zhuhai, China

***Corresponding author: (Yi Yan) yanyi@gig.ac.cn**

Abstract

Interaction between Tethys and the Paleo-Pacific subduction zones in Southeast Asia during the Mesozoic remains poorly understood. Using new and published zircon U-Pb and Hf datasets from Borneo (Paleo-Pacific domain) and Sumatra (Tethyan domain), we propose that isotopically juvenile magmatism was active on both sides of Sundaland due to the initiation of inward-dipping double subduction during the latest Triassic when Indochina collided with Sibumasu, as evidenced by a pronounced positive shift in zircon $\epsilon\text{Hf}(t)$ values from both Cenozoic sedimentary successions and Mesozoic magmatic rocks in Sumatra and Borneo. From the latest Triassic to Cretaceous, the contrasting positive $\epsilon\text{Hf}(t)$ values ranges between Borneo and Sumatra, with Borneo showing a broad range and Sumatra a narrower variability, imply that the inward-dipping double subduction system evolved asymmetrically due to differences in slab dip angles between the subducting Meso-Tethys and Paleo-Pacific oceanic lithosphere. After 80 Ma, this asymmetric double subduction system was disrupted, marked by the complete cessation of arc magmatism in Borneo while isotopically juvenile magmatism continued on Sumatra. Our findings emphasize that, when compared to the contemporary single-sided subduction system of the western Meso-Tethyan domain and the northern Paleo-Pacific domain, SE Asia developed more juvenile crust due to large-scale upper plate extension driven by inward-dipping double subduction.

Plain Language Summary (PLS)

44 The interaction between the Tethyan and Paleo-Pacific domains has shaped the
45 formation of the present megacontinent Eurasia. However, how the two subduction
46 zones (Tethyan and Paleo-Pacific domains) interacted and evolved, and how they
47 impacted on the geology of Southeast Asia is not yet clear. Using radiometric ages
48 and hafnium isotopes from magmatic and detrital zircon, we found that the interaction
49 between the Tethyan and Paleo-Pacific domains in Southeast Asia can be explained by
50 an inward-dipping double subduction model that began in the Late Triassic.
51 Furthermore, our results highlight that the strengthened juvenile crustal signatures in
52 Southeast Asia because the large-scale extension of upper plate in an inward-dipping
53 double subduction system.

54

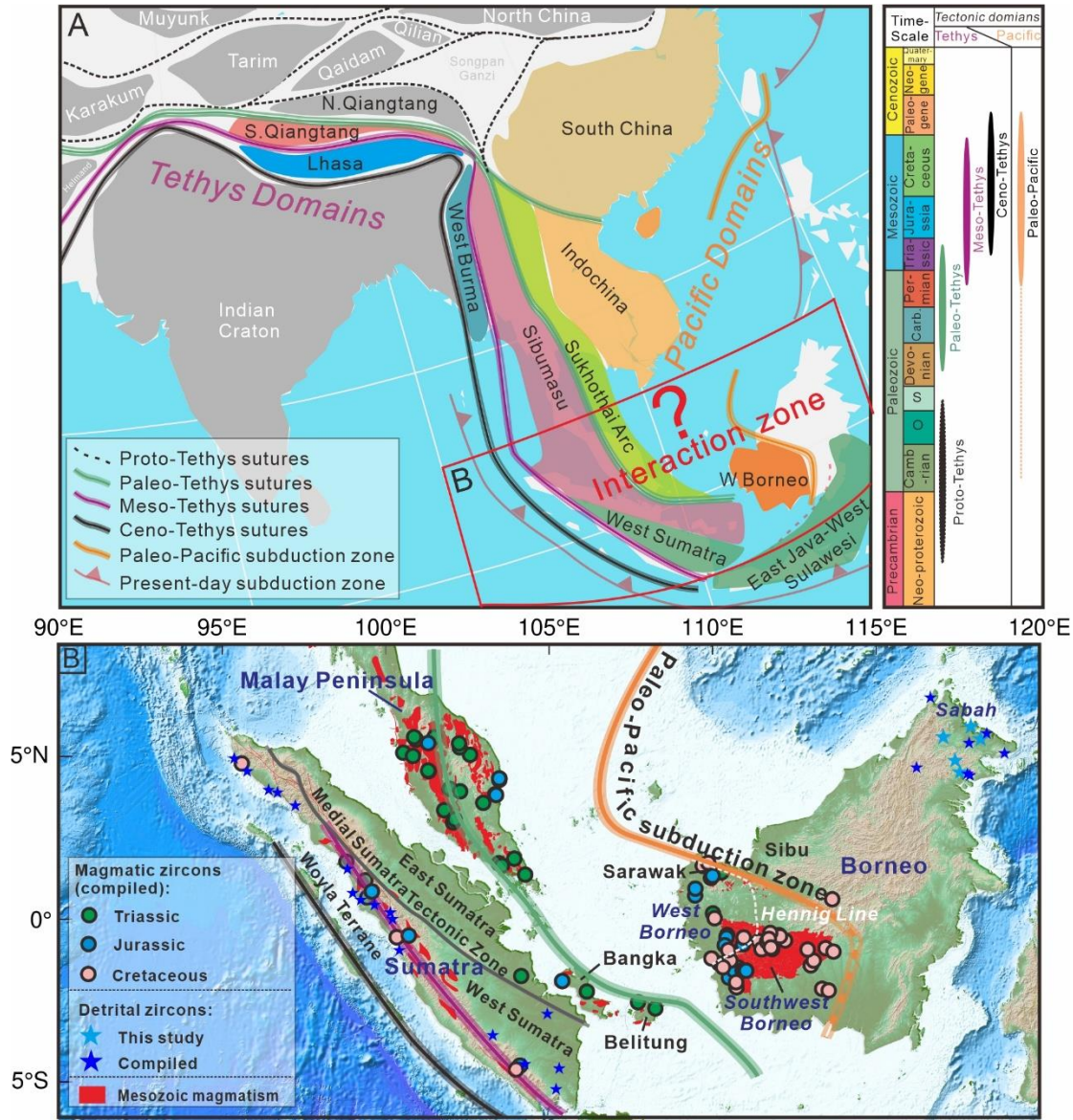
1. Introduction

The last supercontinent cycle was characterized by the breakup of Pangea, a process that began in the Triassic (Olsen, 1997; Golonka, 2007; De Min et al., 2020), leading to the formation of the present megacontinent Eurasia, regarded as a potential precursor to the future supercontinent Amasia (Wang et al., 2020). The assembly of Eurasia was driven by broadly E-W-trending Tethyan-style collisional orogens (Tethyan tectonic domain) and the approximately N-S-trending circum-Pacific-style accretionary orogens (Paleo-Pacific tectonic domain). These trends converge in Southeast Asia, influencing both mantle convection patterns and climate (Metcalf, 2011; Li et al., 2019; Nance et al., 2014; Wang et al., 2020; Wang et al., 2024).

The post Triassic evolution of western Tethyan and the northern Paleo-Pacific tectonic domains have been extensively studied. The western Tethyan tectonic domains are characterized by closure of the Devonian-Triassic Paleo-Tethys in the Late Triassic (Hu et al., 2014; Fan et al., 2024), as well as the subduction and demise of the Permian–Cretaceous Meso-Tethys and Jurassic–Cretaceous Ceno-Tethys, between the Triassic and Paleogene (Hall, 2012; Metcalfe, 2013). These developments were accompanied by the accretion to Eurasia of continental blocks derived from the northern margin of Gondwana (e.g., the South Qiangtang and Lhasa terranes; Fig.1A; Metcalfe, 2017, 2021). In the Phanerozoic the Paleo-Pacific plate has been subducting along the East Asian continental margin in various stages, although the timing of its initial subduction remains debated. For South China,

76 proposed subduction initiation of Paleo-Pacific plate spans from 500 Ma to the
 77 Permian or Triassic (**Fig.1A**; Li and Li, 2007; Isozaki et al., 2010; Zhu et al., 2013;
 78 Pastor-Galán et al., 2021; Zhou et al., 2023), while the North China Craton records
 79 Early Jurassic onset of Paleo-Pacific plate subduction (Wu et al., 2019; Zhu & Xu,
 80 2019; Qiu et al., 2022a, b).

81



83 **Figure 1.** (A) Simplified tectonic map illustrating the Tethys tectonic domains and the
 84 Pacific tectonic domains, along with the temporal evolution of the ocean basins (refer

to [Metcalf 2021; Zhou et al., 2023](#) and reference therein). (B) Location of compiled Mesozoic magmatic and detrital zircons, as well as the new detrital zircons in the interaction zone. Further details are provided in [Table S3](#).

However, the interaction and evolution of these two subduction zones (Tethyan and Paleo-Pacific domains), as well as their impact on the geology of Southeast Asia, remain unclear. Present-day West Sumatra and West and Southwest Borneo, which are separated from the Malay Peninsula by the Sunda Shelf, and the Bangka and Belitung islands, represent the easternmost extent of the Tethyan domain ([Fig 1B; Metcalfe, 2017, 2021; Zhang et al., 2019; Li et al., 2020](#)) and the southernmost extent of the Paleo-Pacific domain ([Metcalf, 1996; Hennig et al., 2017; Breitfeld et al., 2020; Wang et al., 2022a, 2023, 2024](#)). Two principal models have been proposed regarding the origin of Southwest Borneo: (1) it represents an allochthonous terrane that accreted to SE Asia during the Late Jurassic or Early Cretaceous ([Metcalf, 2009; Hall, 2012; Hennig et al., 2017; Breitfeld et al., 2020](#)), or (2) it was autochthonous, undergoing accretion linked to Paleo-Pacific plate subduction since the Earliest Jurassic or possibly earlier ([Wang et al., 2022a, 2023, 2024](#)). Nevertheless, Southwest Borneo—or at least its northwestern portion (the Northwest Schwaner zone, termed West Borneo in [Hennig et al., 2017](#))—was situated along the southeastern margin of the Sundaland continent since the Late Triassic. Tectonic reconstructions constrain accretion of the West Sumatra block onto the Sundaland margin to the Late Triassic,

after which a Mesozoic subduction-related arc developed within a narrow belt throughout West Sumatra (Barber et al., 2005; Cobbing, 2005; Barber & Crow, 2009; Li et al., 2020; Metcalfe, 2021). Thus, the Mesozoic magmatic rocks in West Sumatra and West and/or Southwest Borneo record, respectively, continental accretion and growth related to the northeastward subduction of the Tethyan lithosphere (e.g., Li et al., 2020) and the westward subduction of the Paleo-Pacific plate (Breitfeld et al., 2017, 2020a; Hennig et al., 2017; Wang et al., 2024). These rocks provide an important record for understanding how these two subduction systems interacted.

In this study, we examined compiled regional magmatic and detrital zircon U-Pb data in the West and Southwest Borneo and West Sumatra, and integrated these results with new zircon U-Pb and Hf isotopic data obtained from samples collected across northern Borneo (Sabah). Zircon data from Mesozoic igneous rocks were used to track the spatial distribution of magmatism through time and Mesozoic detrital zircon ages from Upper Oligocene to Neogene sedimentary rocks capture temporal variations in magmatism across the sediment source regions. Collectively, these datasets capture regional temporal and spatial changes in Mesozoic magmatism providing fresh new insights into the tectono-magmatic evolution and underlying geodynamic processes across the interaction zone (Fig 1A) between the Tethyan and Pacific-Pacific domains.

2. Geological Background

Southeast Asia was formed by the successive assembly of different continental fragments that rifted from Gondwana since the Paleozoic (Metcalf, 1988, 2017). During the Triassic, major continental blocks, such as Sibumasu, Indochina, West and SW Borneo were positioned between the Tethyan and Paleo-Pacific domains (Fig.1A; e.g., Metcalf, 2017), herein referred to as the interaction zone of both. The origin of Southwest Borneo remains debated. It may represent either a continental terrane rifted from northwestern Australia (e.g., Metcalf, 2009; Hall, 2012; Hennig et al., 2017; Breitfeld et al., 2020a), or a Paleo-Pacific active continental margin similar or attached to West Borneo (e.g., Wang et al., 2022a, 2023, 2024). In contrast, West Borneo (containing the Northwest Schwaner Zone) was unambiguously situated at the western and southernmost part of the Paleo-Pacific subduction zone in the Triassic, where most of the subduction-related Mesozoic igneous and metamorphic rocks were developed (Fig. 1B; Haile et al., 1977; Williams et al., 1988; Hennig et al., 2017; Breitfeld et al., 2020a). Upper Mesozoic to Paleogene fluvio-deltaic sedimentary rocks and deep-marine turbidites are mainly developed in Sarawak and Sabah, respectively. Sabah, situated at the northern tip of Borneo, is thereby dominated mainly by Paleogene-Neogene clastic sedimentary rocks deposited on the Mesozoic Chert-Spilite Formation/ophiolite basement (Hutchison, 2005). Cenozoic rifting of the Sunda Shelf caused by the propagating South China Sea, along with associated tectonic events in Borneo resulted in erosion and deposition of large volumes of Lower Oligocene to Neogene sediments in Sabah (Hutchison, 1996, 2005; Hall, 2013;

Hall & Breitfeld, 2017; Breitfeld et al., 2023a, b). Although Early Cenozoic drainage reorganization in Borneo triggered dynamic sediment provenance fluctuations between the Malay-Thai Peninsula and West and Southwest Borneo (e.g., Galin et al., 2017; Hennig-Breitfeld et al., 2019; Breitfeld et al., 2020b), most Upper Oligocene to Neogene sedimentary rocks in Sabah are dominated by Cretaceous zircons and were mainly derived by multi-recycling from West and Southwest Borneo with minor inputs from inland Sundaland (e.g., Malay Peninsula) or mainland Asia (van Hattum et al., 2006, 2013; Galin et al., 2017; Hennig-Breitfeld et al., 2019; Breitfeld et al., 2020b, 2023a, b; Quek et al., 2021b). As a result, these Cretaceous zircons-dominant sedimentary successions represent an important archive of continental growth history and magmatism related to subduction of the southernmost Paleo-Pacific oceanic slab beneath Borneo in the Mesozoic.

By contrast, Sumatra lies at the easternmost Tethyan domain and was partly formed from accretion of the Woyla Arc, and the West and East Sumatra blocks in the Cretaceous (Advokaat et al., 2018; Fig. 1B). Rocks exposed in Sumatra record subduction of Mesozoic Tethyan lithosphere following the closure of the Paleo-Tethyan Ocean in the Middle to Late Triassic (Metcalf, 1996; Barber and Crow, 2009). The Woyla Arc is mainly characterized by a Lower Cretaceous volcanic-sedimentary succession, comprising basaltic to andesitic volcanic rocks interbedded with clastic sedimentary units. It is interpreted as an intra-oceanic subduction-related arc that accreted to Sundaland in the Middle-Late Cretaceous due

to the absence of continental rocks (Barber, 2000; Baber et al., 2005; Metcalfe, 2017, 2021). West and East Sumatra are separated by the Medial Sumatra Tectonic Zone, characterized as a major crustal shear zone/strike-slip fault system rather than a suture zone, given the complete absence of exposed ophiolitic components (e.g., Baber & Crow, 2009; Metcalfe 2013). West Sumatra was probably emplaced by the Medial Sumatra Tectonic Zone in the Late Triassic (Baber & Crow, 2009). Triassic-Jurassic and Cretaceous granitoids that represent a subduction-related arc magmatic suite are mainly distributed within a narrow belt in West Sumatra, representing the southeastern extension of the Meso-Tethyan arc system (Gasparon and Varne, 1995; Cobbing, 2005; Zhang et al., 2019; Li et al., 2020). Thus, detrital and magmatic zircon data in West Sumatra record the onset of crustal growth related to subduction of the easternmost Tethyan lithosphere after the Late Triassic (Zhang et al., 2019; Li et al., 2020).

3. Methods

3.1 Sampling and Analytical Methods

A total of five representative sandstones were collected from strata in Sabah (northern Borneo), which include the Cretaceous turbidite slice within the ophiolitic basement (TB-10B), Labang Formation (Late Oligocene, SK-06), Garinono Mélange (Early Miocene, SK-02), Kumaunt Formation (Early Miocene, K-01) and Tanjong Formation (Early-Middle Miocene, K-03). Zircon U-Pb-(Hf) isotopic analyses were

conducted on these samples to constrain temporal variations in magmatism along the southernmost segment of the Paleo-Pacific subduction zone.

Zircon grains were separated using standard density and magnetic techniques after [Mange and Maurer \(1992\)](#). U-Pb dating was performed by laser ablation-inductively coupled plasma-mass spectroscopy (LA-ICP-MS) at Wuhan SampleSolution Analytical Technology Co., Ltd., Wuhan, China using the Agilent 7900 ICP-MS coupled with a GeolasPro laser ablation system. The diameter of the analytical spot is 32 μm . Zircon 91500 (1065 Ma; [Wiedenbeck et al., 1995](#)) and glass NIST610 ([Pearce et al., 1997](#)) served as external standards for U-Pb dating and trace element calibration. Data is provided in [Supplementary Table S1](#).

From the 506 dated grains, 117 concordant zircons with ages younger than 500 Ma were selected for Lu-Hf isotopic analysis by LA-MC (multicollector) ICP-MS to track the Mesozoic tectono-magmatic evolution of Borneo. In-situ Lu-Hf isotopic measurements were performed at Wuhan SampleSolution Analytical Technology Co., Ltd employing a Neptune Plus MC-ICP-MS (Thermo Fisher Scientific, Germany) coupled with a Geolas HD excimer ArF laser ablation system (Coherent, Göttingen). The diameter of the ablation spot is 44 μm . Analyses followed established [Hu et al. \(2012\)](#) operational frameworks. Plešovice, 91500 and GJ-1 are analyzed simultaneously with our samples to ensure the reliability of our data ([Zhang et al. 2020](#)). Their external precision (2SD) is better than 0.000020, with measured values showing concordance with published reference values within analytical uncertainty.

ICPMSDataCal was used to perform off-line selection and integration of analyzed signals and mass bias calibration (Liu et al., 2010). Data is provided in [Supplementary Table S2](#).

3.2 Data Compilation

To determine the interaction and evolution of the two subduction zones (Paleo-Pacific and Tethyan domains), we compiled Neogene detrital zircon U-Pb-(Hf) data from Sabah (Breitfeld et al., 2023a; Zhang et al., 2023) and Sumatra (Hsu, 2016; Zhang et al., 2019). Zircon U-Pb-(Hf) data of Mesozoic magmatic rocks from Sumatra (Li et al., 2020), West Borneo and Southwest Borneo (Setiawan et al., 2013; van Hattum et al., 2013; Hennig et al., 2017; Breitfeld et al., 2017, 2020a; Gan et al., 2022; Qian et al., 2022; Wang et al., 2021a, 2021b, 2022a, 2022b), Indochina (Shellnutt et al., 2013; Tran et al., 2014; Hieu et al., 2015; Shi et al., 2015; Wang et al., 2016; Hou et al., 2019; Nguyen et al., 2019; Minh et al., 2020), Malay Peninsula (Liew & Page et al., 1985; Searle et al., 2012; Ghani et al., 2013; Oliver et al., 2014; Ng et al., 2015; Jamil et al., 2016; Gillespie et al., 2019; Hazad et al., 2019; Cao et al., 2020; Liu et al., 2020; Quek et al., 2021a; Wang et al., 2021a; Yu et al., 2022; Qian et al., 2023), Bangka and Belitung Island (Ng et al., 2017; Wang et al., 2021a) were also compiled.

To ensure data reliability and comprehensiveness, all data were compiled directly from original studies, retaining the authors' own processing approaches—including outlier removal and concordance threshold selection. Compiled data from the

Mesozoic magmatic rocks and the Neogene detrital samples comprising 7,486 zircon U-Pb ages and 4,224 Hf isotopic measurements. The locations of the new study samples and compiled samples are shown in [Figure 1B](#). Compiled zircon age data and Hf isotopic data are shown in [Supplementary Table S3](#) and [Table S4](#), respectively.

4. Results

All new zircon grains from the Cretaceous turbidite slice and Upper Oligocene-Neogene sandstones in Sabah display lengths of 60-200 μm , and axial ratios spanning 1:1 to 3:1 ([Fig. 2](#)). Most of these detrital zircon data yield ages younger than 500 Ma ([Table S1](#)), comprising a total of 114 Paleozoic, 232 Mesozoic and 11 Cenozoic age. Grains exhibit oscillatory zoning ([Fig. 2](#)), and have Th/U ratios > 0.1, consistent with a magmatic origin ([Corfu et al., 2003](#)). The Triassic and Cretaceous zircons display subrounded to euhedral morphologies, suggesting first cycle to moderately recycled input ([Fig. 2](#)).

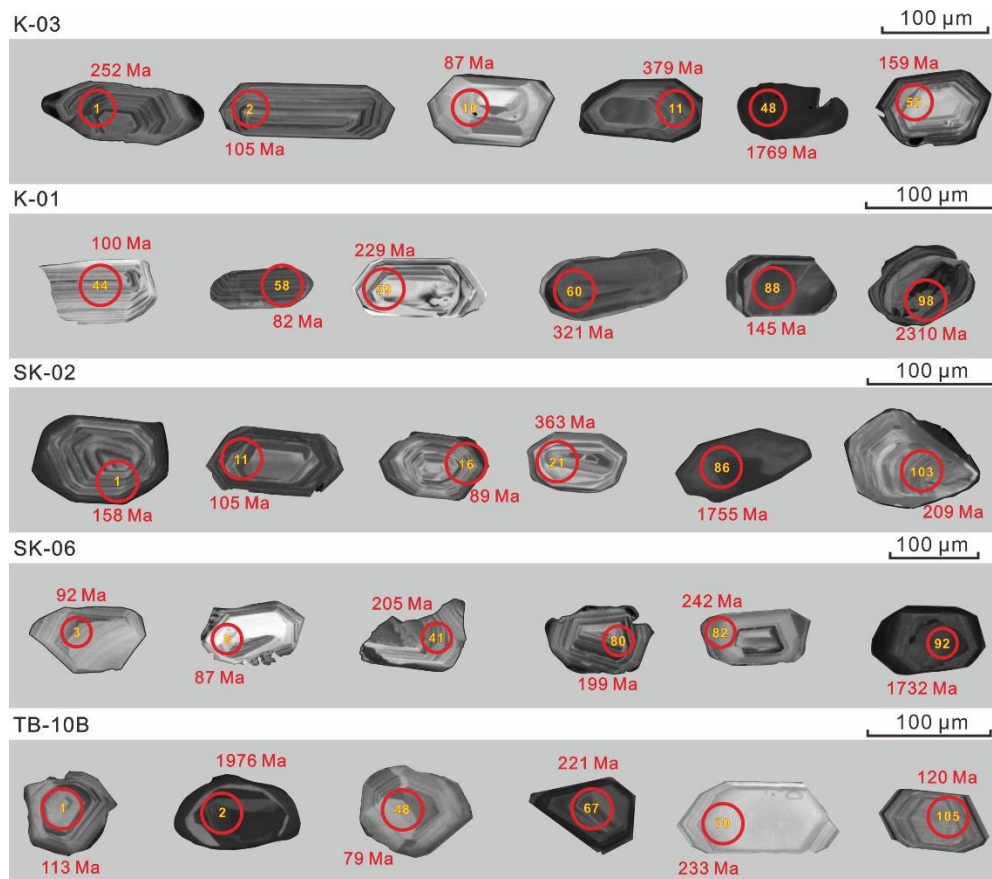
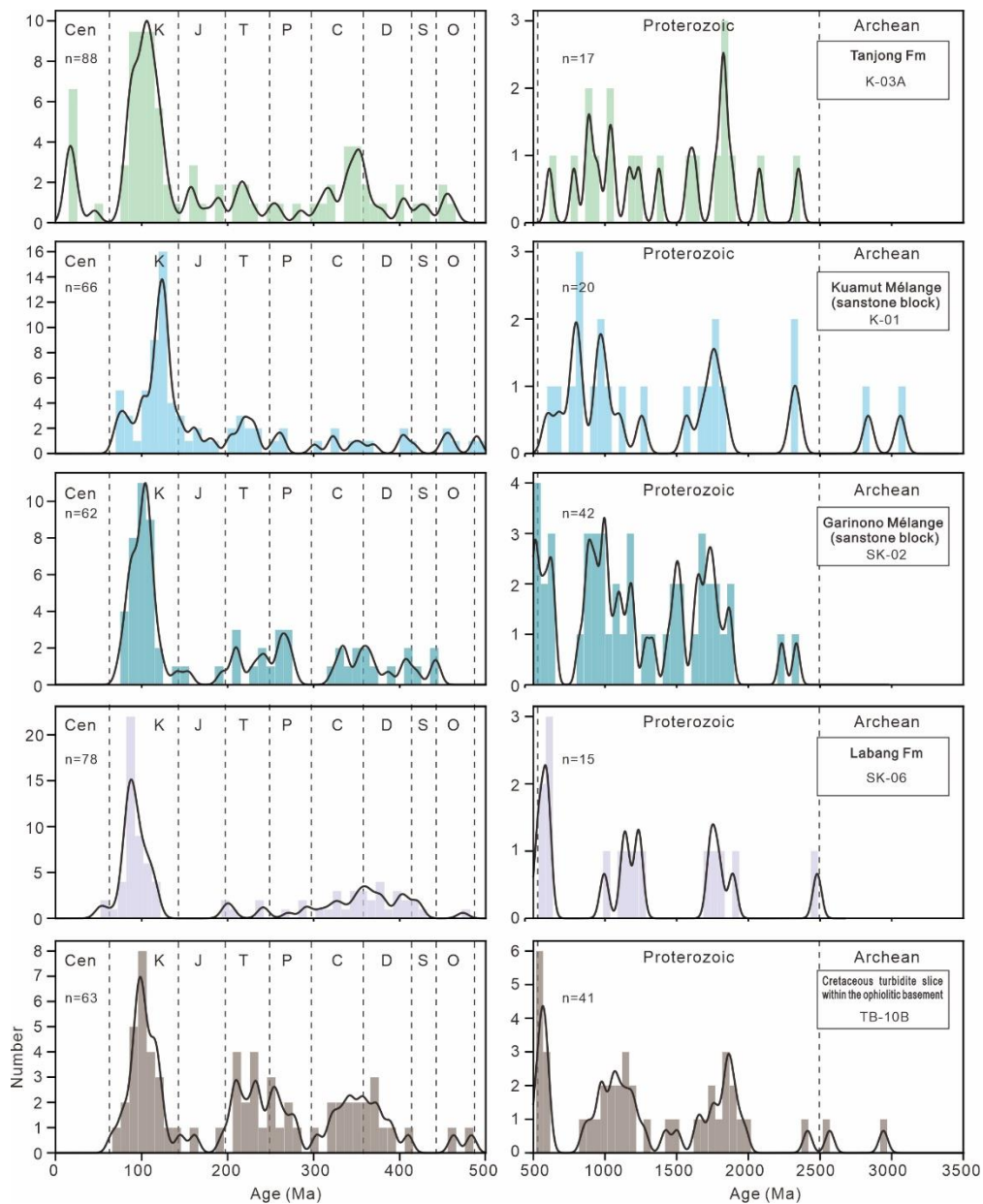


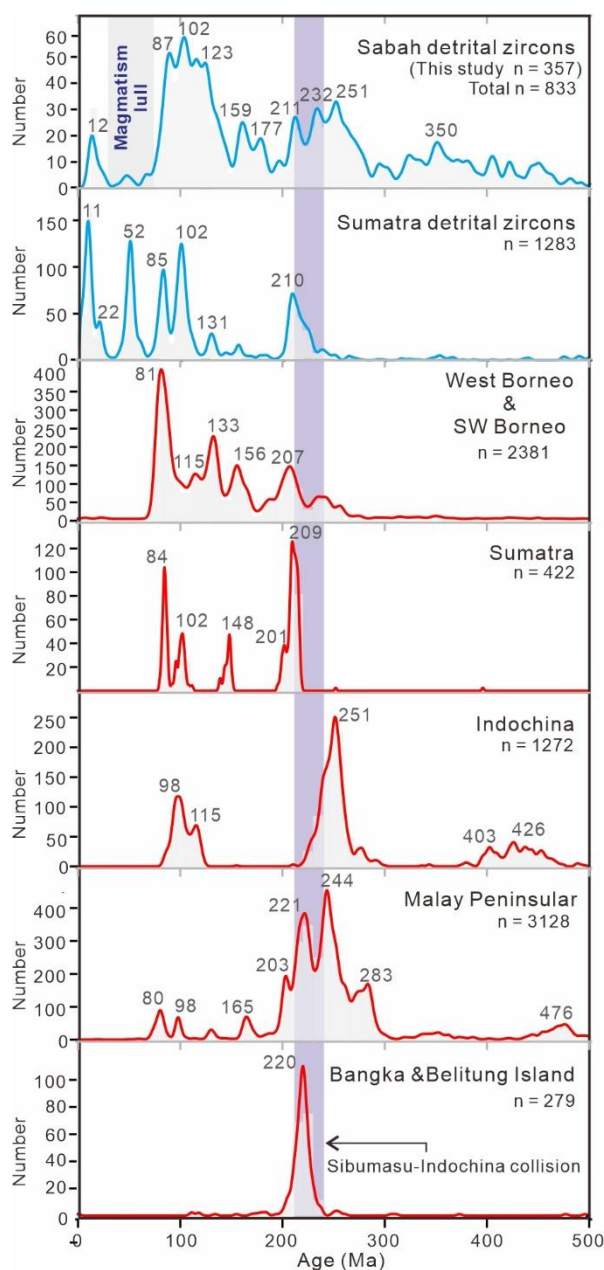
Figure 2. Cathodoluminescent (CL) images of zircons from the Cretaceous turbidite slice and Upper Oligocene-Neogene sandstones sampled in this study.

The five samples exhibit comparable zircon age distributions, while the Cretaceous turbidite slice within the ophiolitic basement (TB-10B) contains a higher abundance of Permo-Triassic and Devonian-Carboniferous zircons (Fig. 3). A limited population of Oligocene to Early Miocene zircons exists in K-03A of Tanjong Formation, documenting potential magmatism associated with Proto-South China Sea subduction during this interval (e.g., Breitfeld et al., 2023a). When integrated with detrital zircons from published Neogene sedimentary rock samples in Sabah (e.g., Breitfeld et al., 2023a; Zhang et al., 2023), these zircons maintained a distribution

257 pattern dominated by Late Cretaceous (~100 Ma) ages, while the Kernel Density
 258 Estimate (KDE) plots show minor age peaks in the Permo-Triassic (~210–260 Ma)
 259 and Devonian-Carboniferous (~330–380 Ma; **Fig. 4**). The $\varepsilon\text{Hf}(t)$ values of these
 260 detrital zircons from five samples began to increase in the Latest Triassic, and became
 261 overwhelmingly positive during the Jurassic and Cretaceous ($\varepsilon\text{Hf}(t) = -5.2 \sim +14.9$;
 262 **Fig. 5**)



265 **Figure 3.** Kernel density estimation (KDE) spectra of detrital zircons from the
 266 Cretaceous turbidite slice and Upper Oligocene-Neogene sandstones sampled in this
 267 study.
 268



269
 270 **Figure 4. (A)** Kernel density estimation (KDE) spectra of published zircon U-Pb ages
 271 of Mesozoic magmatic rocks around Sundaland. New and compiled detrital zircons
 272 U-Pb ages from the Upper Oligocene-Neogene sedimentary rocks in Sabah and

Sumatra are also shown for comparison. For the references pertaining to the compiled dataset, please refer to the Methods section. [Supplementary Table S1](#) and [Table S3](#) present the new and compiled zircon age data, respectively.

[Figure 5](#) shows magmatic activity across West Sumatra and West and Southwest Borneo from the Permian, through the Triassic when Sibumasu collided with Indochina, to Early Miocene. Prior to the latest Triassic, magmatic zircons are scarce in both Borneo and West Sumatra. However, their detrital zircons exhibit scattered $\epsilon\text{Hf}(t)$ values, with detrital zircons from West Sumatra showing more positive $\epsilon\text{Hf}(t)$ values relative to those from West and Southwest Borneo. After the latest Triassic, on the western side (West Sumatra), magmatic zircons exhibit a narrow range in positive ϵHf values whereas detrital zircons show a progressive trend towards increasingly positive ϵHf values. This is not seen in the West and Southwest Borneo data, which instead shows a wider scattering of positive ϵHf values since the latest Triassic. Subduction-related magmatism in the West and Southwest Borneo appears to have ceased for a considerable period following 80 Ma. By contrast detrital zircon data from West Sumatra imply ongoing magmatism and a continuation of the trend of increasing positive ϵHf values.

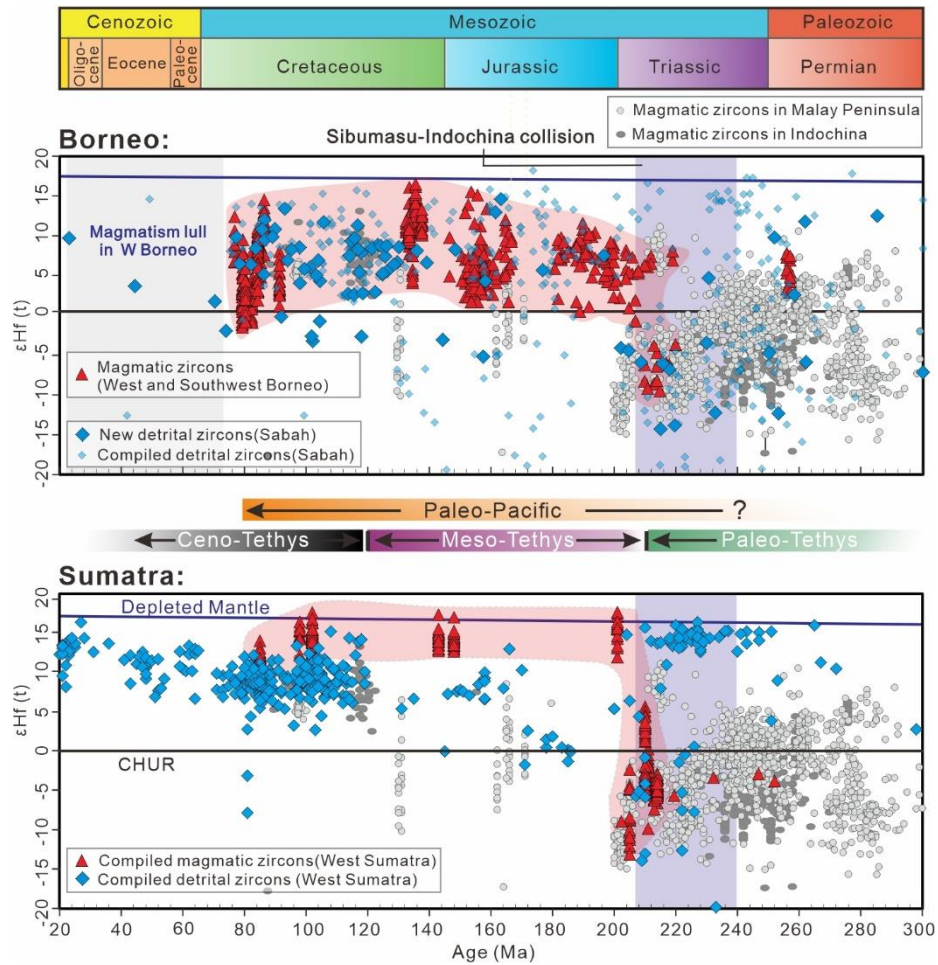


Figure 5. Zircon ages vs. zircon $\epsilon_{\text{Hf}}(t)$ values of the Mesozoic magmatic rocks and Neogene sedimentary rocks in West Sumatra and Borneo. Magmatic zircons compiled from Mesozoic igneous rocks in the Malay Peninsula are also shown for comparison. For the references pertaining to the compiled dataset, please refer to the Methods section. [Supplementary Table S2](#) and [Table S4](#) present the new and compiled zircon Hf isotope data, respectively.

4. Discussion

4.1. Upper Oligocene-Neogene Sediments in Sabah: A Record of Magmatism in the Southern Pacific-Pacific Domain

Previous provenance analyses indicates that sources of Cenozoic sedimentary rocks preserved in Sarawak and Sabah are mainly from West Borneo, Southwest Borneo and the Malay Peninsula with some grains may have been recycled from older sedimentary rocks (e.g., [van Hattum et al., 2013](#); [Galin et al., 2017](#); [Hennig-Breitfeld et al., 2019](#), [Breitfeld et al., 2020b, 2023a, b](#)). The Malay Peninsula mainly provided Permian-Triassic zircons, while West Borneo yielded Triassic and Cretaceous zircons, and Southwest Borneo dominantly supplied Cretaceous age grains ([Fig. 4](#)). New detrital zircon data from Upper Oligocene-Neogene sandstones are also dominated by Cretaceous ages ([Fig. 3](#)), suggesting that sediment was mainly sourced from West Borneo and Southwest Borneo via the proto-Rajang River drainage system by recycling or directly from the arc, rather than from the Malay Peninsula (e.g., [Breitfeld et al., 2020b](#)). The subrounded to euhedral morphological signatures of Triassic zircons indicate that they may directly originate from the Triassic magmatic rocks of West Borneo ([Fig. 2](#)), while sedimentary recycling of the Kuching-Sibu zone incorporating Malay-Thai and West Borneo provenance components remains a plausible mechanism (e.g., [Breitfeld et al., 2020b; 2023a, b](#)). Similar to the KDE age spectra, an MDS plot ([Fig. 6](#); [Vermeesch et al., 2016](#)) also shows zircon age distributions from Sabah samples plotting closest to zircon ages from magmatic rocks of West Borneo and Southwest Borneo, suggesting that this was the primary source area.

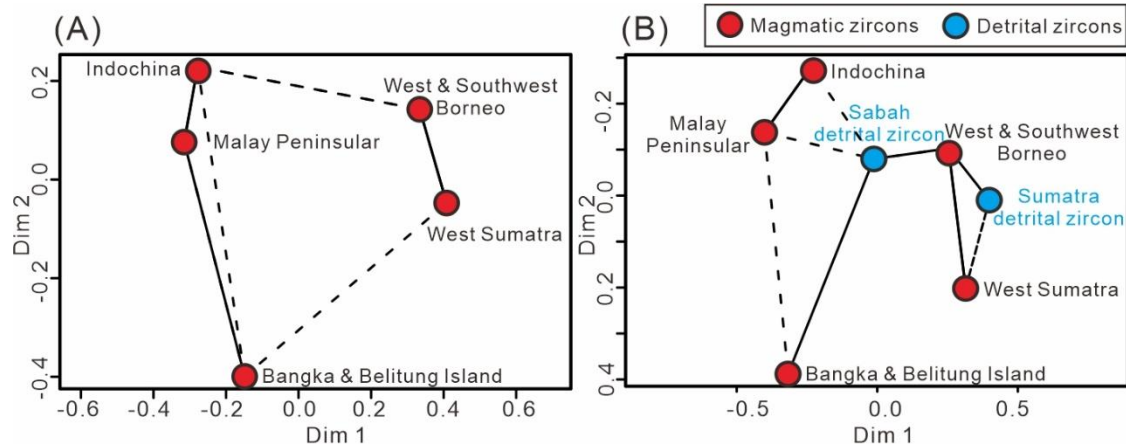


Figure 6. A Multi-Dimensional Scalar (MDS; Vermeesch et al., 2016) plot for compiled zircon U-Pb ages from Mesozoic magmatic rocks around Sundaland, (A) with or (B) without the new and compiled Neogene detrital zircon data in Borneo and Sumatra. For the references pertaining to the compiled dataset, please refer to the Methods section.

Magmatism in West Borneo and Southwest Borneo has been recognized as divided into Triassic and Jurassic subduction-related magmatic episodes and a Cretaceous magmatic arc associated with the Paleo-Pacific plate subduction (Williams et al., 1988; Breitfeld et al., 2017, 2020a; Hennig et al., 2017; Wang et al., 2021, 2022a, 2024), while some Early Jurassic rift-related within-plate magmatism also developed in Southwest Borneo (Breitfeld et al., 2020a). Zircon $\epsilon\text{Hf}(t)$ values serve as a powerful tracer for sediment provenance (e.g., Zhang et al., 2023), with their capacity to distinguish between mantle-derived material (more positive) and older crustal components (characterized by strongly negative $\epsilon\text{Hf}(t)$ values) providing critical insights into the relative contributions of these endmembers to magmatic

339 systems (Sundell & Macdonald, 2022). Most detrital zircons younger than 200 Ma
340 have $\epsilon\text{Hf}(t)$ values similar to those of West Borneo and Southwest Borneo magmatic
341 rocks (Fig. 5), and consistent with the implications of the KDEs and MDS plots that
342 suggest a dominant supply from West Borneo and Southwest Borneo. A scarcity of
343 detrital zircons postdating ~80 Ma aligns with the waning and cessation of
344 subduction-related magmatic activity in West Borneo and Southwest Borneo
345 (Williams et al., 1988; Hennig et al., 2017; Breitfeld et al., 2017, 2020a; Wang et al.,
346 2024). A small number of zircons younger than 200 Ma fall within the $\epsilon\text{Hf}(t)$ range of
347 granites in the Malay Peninsula, indicating limited input from that area (e.g., Breitfeld
348 et al., 2020b). The $\epsilon\text{Hf}(t)$ values of our detrital zircons from Sabah, that represent an
349 archive of magmatism across West Borneo and Southwest Borneo, began to increase
350 in the Latest Triassic, and became overwhelmingly positive during the Jurassic and
351 Cretaceous (Fig. 5). The compiled magmatic zircons from West Borneo and
352 Southwest Borneo also have heterogeneous $\epsilon\text{Hf}(t)$ values (varying by up to ~20 ϵ
353 units) in the Latest Triassic, followed by fully positive $\epsilon\text{Hf}(t)$ values with juvenile
354 features (Fig. 5). Although the detrital zircons in the Upper Oligocene-Neogene strata
355 was interpreted as multi-recycling products from Rajang Group and/or Crocker
356 Formation (Hennig-Breitfeld et al., 2019; Breitfeld et al., 2020b, 2023a, 2023b), the
357 close similarity of results between Sabah and West and Southwest Borneo supports
358 the view that the Neogene sediments in Sabah effectively document the temporal
359 changes in magmatic activity in West Borneo and Southwest Borneo since the

Mesozoic, thus serving as a record of the magmatic evolution of the southern
Paleo-Pacific domain.

4.2. Spatiotemporal Evolution of Magmatism in each Subduction System

Published whole-rock elemental and Sr-Nd-Pb-(Hf-O) isotopic results indicate
that the Mesozoic magmatic rocks in West Borneo were the products of subduction of
the Paleo-Pacific plate under the East Asia active continental margin (Wang et al.,
2021; 2022a; 2024), while some Jurassic magmatic rocks in Southwest Borneo are
interpreted as rift-related within-plate granites (Breitfeld et al., 2020a). Mesozoic
granitoids in Sumatra represent the products of subduction magmatism in the
easternmost Tethys (Li et al., 2020). Temporally, Mesozoic magmatism in West
Borneo and Southwest Borneo exhibits some similarities in age with Sumatra, as
shown by the magmatic zircon U-Pb ages on the KDE and MDS plots (Fig. 4, 6).
During the Early Permian to Middle Triassic, magmatism associated with
Paleo-Tethyan subduction predominantly occurred in East Malaysia, exhibiting
distinct negative $\epsilon_{\text{Hf}}(t)$ signatures (Fig. 5, e.g., Ng et al., 2015; Gillespie et al., 2019;
Liu et al., 2020; Wang et al., 2021a). The positive $\epsilon_{\text{Hf}}(t)$ values of detrital zircons
from Sumatra likely preserve information predating its accretion to Sundaland, given
that Sumatra may represent the southern extension of the West Burma block (Barber
& Crow, 2009; Metcalfe, 2013). In contrast, westward subduction of the Paleo-Pacific
plate remained limited or inactive until the Late Triassic (e.g., Zhou et al., 2023).

381 Therefore, only sporadic magmatism from this period is preserved in West Sumatra
382 and West Borneo ([Fig. 5](#)). Since latest Triassic, the temporal trends in Hf isotope
383 variations are broadly similar in magmatic and detrital zircons from both Sumatra and
384 Borneo, although $\epsilon\text{Hf}(t)$ values of magmatic and detrital zircons in Sumatra are
385 consistently higher and more uniform than those in Borneo from the same period ([Fig.](#)
386 [5](#)). This suggests that evolution of the Mesozoic magmatic arc was temporally
387 synchronous across the two active continental margins (Sumatra and Borneo). The
388 notable variation (~ 20 ϵ units) in $\epsilon\text{Hf}(t)$ values seen in latest Triassic magmatic and
389 detrital zircons (220–200 Ma) from both Sumatra and Borneo, representing the
390 western and eastern boundaries of Sundaland, suggest a mix of evolved and juvenile
391 crust in each subduction system immediately after Triassic collision between
392 Indochina and Sibumasu. A trend to positive $\epsilon\text{Hf}(t)$ values on Borneo and Sumatra
393 was established during the Jurassic and Cretaceous, indicating that juvenile crustal
394 growth is prevalent on both sides of the interaction zone ([Fig. 5](#)). In the central part of
395 the overriding plate (Malay Peninsula), magmatic rocks remain isotopically evolved,
396 implying that far from the trench the continental mantle lithosphere is thick (e.g.,
397 [Chapman et al., 2017](#)). Detrital data show a magmatic lull after ~ 80 Ma in West and
398 Southwest Borneo, indicating that subduction-related arc magmatism in West and
399 Southwest Borneo had largely ceased by that time ([Hennig et al., 2017](#); [Breitfeld et al.,](#)
400 [2020a](#)), unlike Sumatra where magmatism continued throughout the Cenozoic ([Fig. 4,](#)
401 [5](#)).

402 Spatially, the post-Latest Triassic magmatic rocks of West Sumatra are distributed
403 along a narrow belt near the trench with high and uniformly positive $\epsilon\text{Hf}(t)$ values,
404 while those in West and Southwest Borneo are relatively more widely distributed with
405 lower positive $\epsilon\text{Hf}(t)$ values away from the trench ([Fig. 1B, 7A](#)), potentially due to
406 differences in the angle, age, and rate of the subducting plates. Although plate
407 kinematics are not well-constrained due to a lack of preserved oceanic lithosphere,
408 reconstructions of global plate motion show that from the Jurassic to the Cretaceous,
409 there is no consistent pattern in reconstructed convergence rates between the two
410 margins of Sundaland ([Fig. 7B; Müller et al., 2016](#)), this suggests that convergence
411 rate is not the primary factor influencing the spatial distribution patterns of Mesozoic
412 magmatic rocks. However, global plate reconstructions predict the eastern margin of
413 interaction zone was mainly influenced by subduction of older Paleo-Pacific oceanic
414 lithosphere that would be consistent with accreted ocean plate stratigraphy ages in SW
415 Hokkaido, Japan ([Ishiga and Ishiyama, 1987](#)). By contrast, West Sumatra initially
416 experienced subduction of relatively younger oceanic lithosphere that separating it
417 from the Woyla Arc ([Advokaat et al., 2018](#)). Subduction of more steeply dipping
418 young oceanic lithosphere would tend to form a narrow arc near the trench due to
419 their weaker ability to carry volatiles to the lower crust, compared to more gently
420 dipping subduction of a colder and older serpentinized Paleo-Pacific oceanic
421 lithosphere (e.g., [Bastias-Silva et al., 2024](#)).

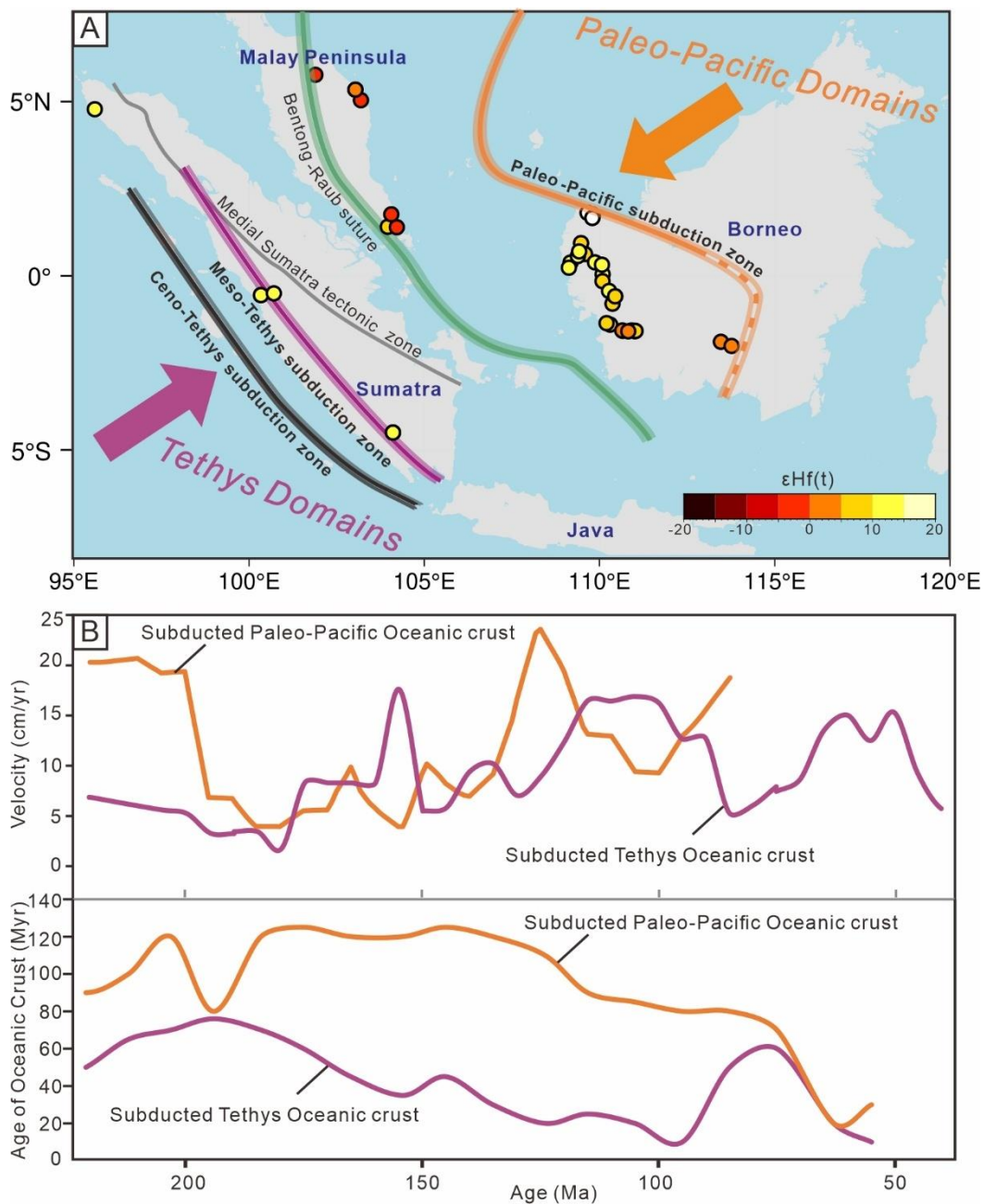


Figure 7. (A) Spatial distribution of zircon $\epsilon\text{Hf}(t)$ values Mesozoic magmatic rocks (200–66 Ma) in West Sumatra, Malay Peninsula, and West and Southwest Borneo. Filled circles represent the mean $\epsilon\text{Hf}(t)$ values of magmatic zircons. (B) Convergence rate and oceanic plate age along the two subduction zones of Sundaland (orange line=Paleo-Pacific; blue=Tethyan) based on global plate reconstructions of Müller et al. (2016, 2019).

429

430 **4.3. Inward Dipping Double Subduction Initiated in Latest Triassic**

431 Spatiotemporal variations in radiogenic isotope compositions can shed light on
432 the evolution of subduction zone dynamics. In Sumatra, a fundamental restructuring
433 of the arc system in the Latest Triassic is identified based on the marked increase in
434 $\epsilon\text{Hf}(t)$ values observed in zircons from Mesozoic granitoids, as well as detrital zircons
435 from Cenozoic strata and modern river sediments ([Fig 5; Zhang et al., 2019; Li et al.,](#)
436 [2020](#)). An extensional fringing arc related to NW-SE trending extensional basins in
437 Sumatra ([Barber and Crow, 2009](#)) or slab retreat or rollback that occurred shortly after
438 the Middle-Late Triassic collision of Sibumasu with Indochina and East Malaya, have
439 been considered as indicative of the initial input of juvenile material in Sumatra ([Li et](#)
440 [al., 2020](#)).

441 For Borneo, the presence of Mesozoic supra-subduction zone ophiolites and
442 Mesozoic-Cenozoic basin indicates that Borneo has been subjected to a protracted
443 extensional setting since the Late Triassic ([Burton-Johnson et al., 2023](#)). The
444 development of the Triassic Sadong and Kuching Formations and Cretaceous
445 Pedawan Formation—characterized by forearc basin successions in West
446 Borneo—provides critical evidence for syn-depositional extensional tectonics ([Pieters](#)
447 [et al., 1993; Breitfeld et al., 2017, 2023c; Mazumder et al., 2021](#)), likely associated
448 with episodic slab rollback during subduction of the Paleo-Pacific plate ([Zhou et al.,](#)
449 [2023](#)). Significant extensional collapse around 215 Ma also characterizes the

Sibumasu terrane, particularly in northern Thailand and potentially other regions (Morley, 2018). Therefore, the notable variation (220–200 Ma, ~20 ϵ units) in magmatic and detrital zircon ϵ Hf(t) values from both Sumatra and Borneo suggest the addition of juvenile material in an extensional setting in each subduction system.

The initiation of double subduction is usually associated with collision, such as the Solomon subduction zone (Sun et al., 2021). Numerical modelling indicates that during the early stages of a double subduction system, the stress on the overriding plate either remained in an extensional state (Lyu et al., 2019) or transitioned from compression to extension, typically within the first few million years (Zhang et al., 2024). Therefore, we consider that an inward-dipping double subduction system underneath Sundaland (the interaction zone) began to be established immediately after latest Triassic collision between Indochina and Sibumasu (Fig. 8).

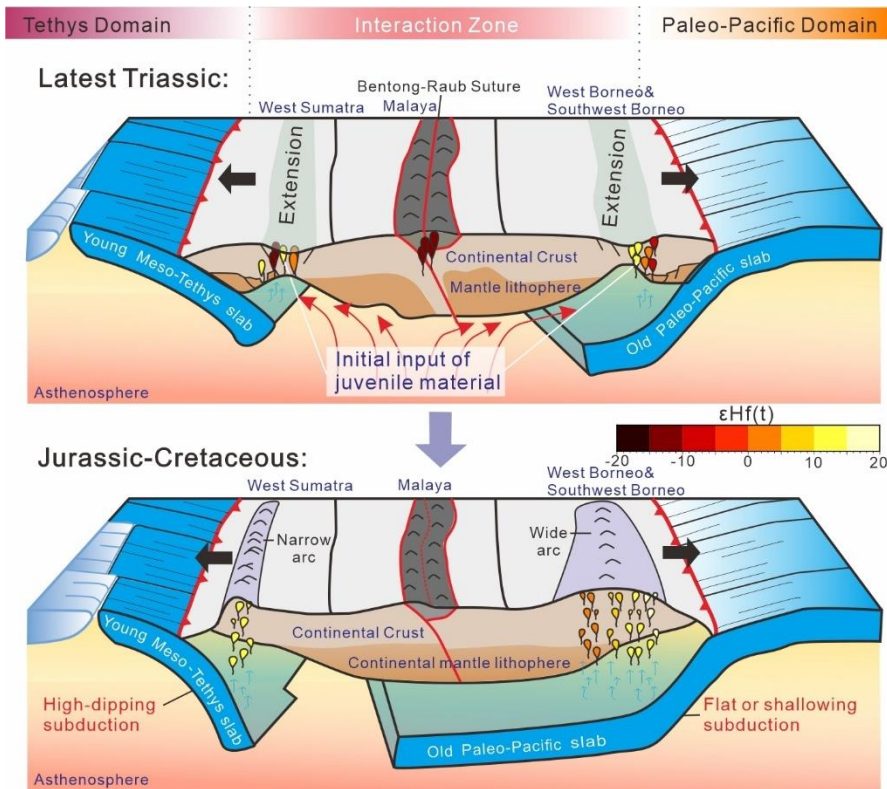


Figure 8. Input of juvenile material into Sumatra and Borneo, initiated in the Latest Triassic and continued to develop from the Jurassic to the Cretaceous due to the extension of the inward-dipping double subduction.

During the Jurassic and Cretaceous, the positive $\epsilon\text{Hf}(t)$ values on Borneo and Sumatra indicate that the melt source region of the two subduction zones is predominantly depleted asthenospheric mantle but, mixed with varying proportions of isotopically evolved continental lithospheric mantle. The contrasting ranges of positive $\epsilon\text{Hf}(t)$ values imply the double subduction system evolved asymmetrically. The narrow spatial distribution observed in the arc magmatism of Sumatra and their uniformly positive $\epsilon\text{Hf}(t)$ isotopic values is thus attributed to the absence of continental lithospheric mantle near the trench during the high-angle subduction of the Meso-Tethys slab (e.g., [Chapman et al., 2017](#)). In contrast, the wide arc magma belt and broader Hf isotopic values in Borneo represent varying degrees of involvement of continental mantle lithosphere during more shallow dipping subduction of the Paleo-Pacific oceanic crust in that time ([Zhou et al., 2023](#); **Fig. 8**). Around 80 Ma, this stable asymmetric double subduction system was disrupted, marked by the complete cessation of subduction-related arc magmatism in Borneo while magmatism continued in West Sumatra. In SE Vietnam (north of West Borneo) subduction-related magmatism had also ceased by c. 80 Ma ([Hennig-Breitfeld et al., 2021](#)), implying the waning of the Paleo-Pacific subduction zone at that time. The

magmatic arc in West Sumatra has maintained isotopically juvenile signals even after 80 Ma (**Fig. 5**). This aligns with numerical models suggesting that large-scale extension, along with extensive and vigorous mantle upwellings, persists even after one of the two subductions ceases (**Li et al., 2024**).

4.4. Juvenile Crust Production in SE Asia Linked to Double Subduction

Our data show a significant isotopic shift from isotopically evolved to isotopically juvenile in the continental arc of the Sundaland margin around 200 Ma, triggered by collision between Sibumasu and Indochina and the initiation of an inward-dipping double subduction regime (**Fig. 5**). During the latest Triassic to Jurassic, Southeast Asia served as an interaction zone connecting the Qiangtang block of western Meso-Tethys and South China of the northern Paleo-Pacific, where single subduction developed (**Fig. 9A**). However, isotopic data for contemporary batholith from South Qiangtang in the Meso-Tethys domain and South China in the Paleo-Pacific domain exhibit $\epsilon_{\text{Hf}}(t)$ values lower than those measured from West and Southwest Borneo and West Sumatra in the interaction zone (**Fig. 9B**). This raises the possibility that, compared to single subduction in the Meso-Tethys or Paleo-Pacific domains, an inward-dipping double subduction system is more conducive to the formation of juvenile crust.

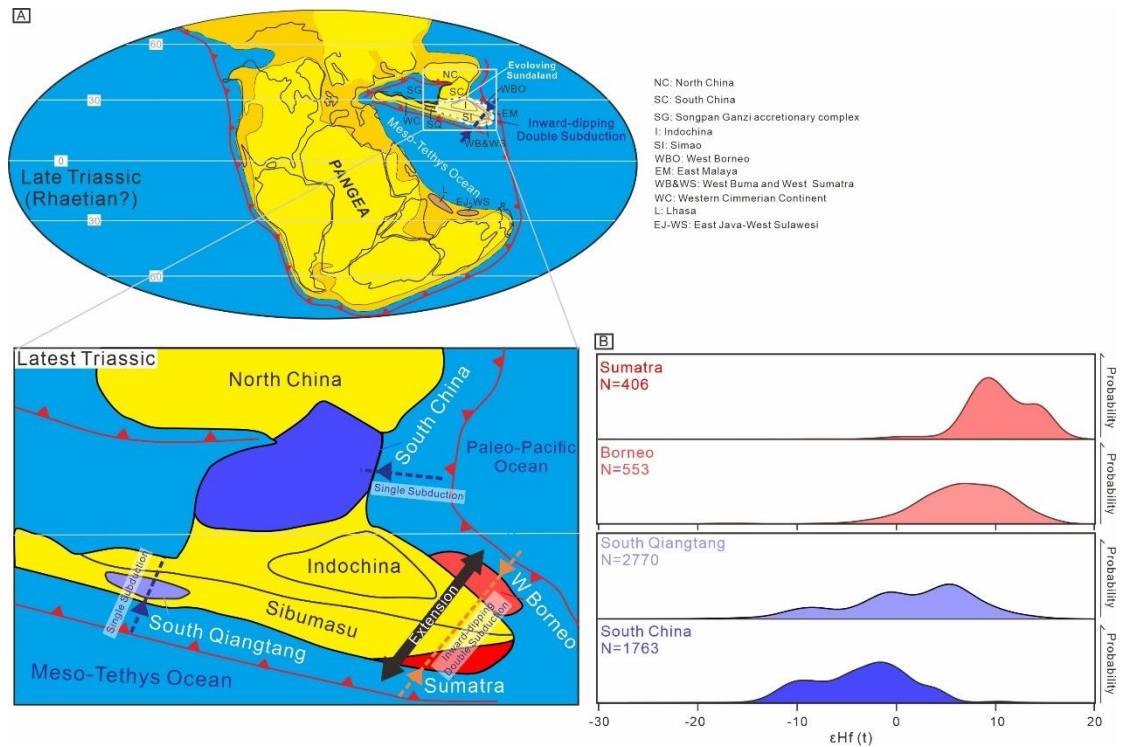


Figure 9. (A) Palaeogeographic reconstructions for the Paleo-Pacific and Eastern Tethys in late Triassic (after Metcalfe, 2017). Notes the enlarged view of the interaction zone. (B) Density curves of $\epsilon Hf(t)$ from latest Triassic to early Late Cretaceous (200–80 Ma) for batholith in the Tethys and Paleo-Pacific domains. Data of batholith in the South Qiangtang and South China are from Gong et al. (2024), Zhang et al. (2023) and references therein.

Numerical simulations indicate that inward-dipping double subduction results in larger-scale upper plate extension and greater volumes of upwelling mantle compared to single subduction (Lyu et al., 2019; Li et al., 2024; Zhang et al., 2024). This fits with evidence of widespread extension across Sumatra and Borneo (Barber and Crow, 2009; Pieters et al., 1993; Breithfeld et al., 2017, 2023c; Mazumder et al., 2021; Burton-Johnson et al., 2023; Zhou et al., 2023). Isotopically juvenile signature in

Sumatra persist to the present day (**Fig. 5**) and may be a residual feature inherited from the time of double subduction (e.g., [Li et al., 2024](#)). Our study emphasizes that the role of inward-dipping double subduction in Southeast Asia, including its influence on mantle structure and temperature.

5. Conclusions

Records of magmatic and detrital zircons from both Borneo and Sumatra show an inward-dipping double subduction system beneath Sundaland initiated in the latest Triassic, coinciding with the collision of Indochina and Sibumasu. Magmatism persisted on both West and Southwest Borneo and West Sumatra from the latest Triassic to the Cretaceous; however, it evolved asymmetrically due to differences in the subducting oceanic lithospheres—specifically, the younger, steeply dipping Meso-Tethys and the older, more shallowly dipping Paleo-Pacific oceanic lithosphere. After 80 Ma, subduction-related magmatism on the Borneo side ceased following the termination of subduction of Paleo-Pacific oceanic crust, while on the Sumatra side, magmatism with isotopically juvenile compositions continued. Furthermore, our study establishes a possible causal link between the strengthened juvenile crustal signatures in Southeast Asia and the large-scale extension of the overriding lithospheric plate in an inward-dipping double subduction system.

Acknowledgments

This work was funded by the National Key Research and Development Program of China (2023YFF0803403), the Strategic Priority Research Program (B) of the Chinese Academy of Sciences (XDB0840200), the National Natural Science Foundation (42202248), the Guangdong Basic and Applied Basic Research Foundation (2023A1515011786) of China and the Director General's Scientific Research Fund of Guangzhou Marine Geological Survey, China (2023GMGSJZJJ00007). We are grateful to the Editor Margaret Rusmore, the Associate Editor, an anonymous reviewer and H. Tim Breitfeld for their careful and constructive reviews on our paper.

Open Research

The [Supporting Information](https://doi.org/10.17632/8g669bt2bt.1) and [Table S1-S4](#) is available at <https://doi.org/10.17632/8g669bt2bt.1> (Zhao, 2025).

References

- Advokaat, E. L., Bongers, M. L. M., Rudyawan, A., BouDagher-Fadel, M. K., Langereis, C. G., & van Hinsbergen, D. J. J. (2018). Early Cretaceous origin of the Woyla Arc (Sumatra, Indonesia) on the Australian plate. *Earth and Planetary Science Letters*, 498, 348-361. <https://doi.org/10.1016/j.epsl.2018.07.001>
- Barber, A.J., Crow, M.J., Milsom, J.S. (2005). Sumatra: Geology, Resources and Tectonic Evolution, 31. Geological Society [London] Memoir, p. 290.
- Barber, A.J., & Crow, M.J. (2009). Structure of Sumatra and its implications for the tectonic assembly of Southeast Asia and the destruction of Paleotethys. *The*

561 *Island Arc*, 18(1), 3–20, <https://doi.org/10.1111/j.1440-1738.2008.00631.x>

562 Bastias-Silva, J., Burton-Johnson, A., Chew, D., Riley, T., Jara, W., & Chiaradia, M.

563 (2024). A temporal control on the isotopic compositions of the Antarctic

564 Peninsula arc. *Communications Earth & Environment*, 5(1), 157.

565 <https://doi.org/10.1038/s43247-024-01301-1>

566 Bataille, C. P., Willis, A., Yang, X., & Liu, X. M. (2017). Continental igneous rock

567 composition: A major control of past global chemical weathering. *Science*

568 *Advance*, 3(3), e1602183. <https://doi.org/10.1126/sciadv.1602183>.

569 Breitfeld, H. T., Hall, R., Galin, T., Forster, M. A., & BouDagher-Fadel, M. K. (2017).

570 A Triassic to Cretaceous Sundaland–Pacific subduction margin in West Sarawak,

571 Borneo. *Tectonophysics*, 694, 35–56. <https://doi.org/10.1016/j.tecto.2016.11.034>

572 Breitfeld, H. T., Davies, L., Hall, R., Armstrong, R., Forster, M., Lister, G., Thirlwall,

573 M., Grassineau, N., Hennig-Breitfeld, J., & van Hattum, M. W. A. (2020a).

574 Mesozoic Paleo-Pacific Subduction Beneath SW Borneo: U-Pb Geochronology

575 of the Schwaner Granitoids and the Pinoh Metamorphic Group. *Frontiers in*

576 *Earth Science*, 8. <https://doi.org/10.3389/feart.2020.568715>

577 Breitfeld, H. T., Hennig-Breitfeld, J., BouDagher-Fadel, M. K., Hall, R., & Galin, T.

578 (2020b). Oligocene-Miocene drainage evolution of NW Borneo: Stratigraphy,

579 sedimentology and provenance of Tatau-Nyalau province sediments. *Journal of*

580 *Asian Earth Sciences*, 195, 104331. <https://doi.org/10.1016/j.jseaes.2020.104331>

581 Breitfeld, H. T., Hall, R., Suggate, S. M., van Hattum, M. W. A., Hennig-Breitfeld, J.,

582 BouDagher-Fadel, M. K., Webb, M., & Franzel, M. (2023a). Neogene
583 sedimentary successions in northern and central Sabah: Provenance and tectonic
584 implications. In *Stratigraphy of Geo- and Biodynamic Processes* (pp. 71-119).
585 <https://doi.org/10.1016/bs.sats.2023.08.009>

586 Breitfeld, H. T., Hennig-Breitfeld, J., Anthony, G., BouDagher-Fadel, M., Vermeesch,
587 P., Lünsdorf, K., Rösel, D., Konrad-Schmolke, M., & Gilbricht, S. (2023b). The
588 onshore West Baram Delta deposits: Provenance and drainage in the Middle
589 Miocene to Pliocene in NW Borneo and comparison to the Champion Delta.
590 *Marine and Petroleum Geology*, 158, 106537.
591 <https://doi.org/10.1016/j.marpetgeo.2023.106537>

592 Breitfeld, H. T., Burley, S. D., Galin, T., Hennig-Breitfeld, J., & Rajali, R. (2023c).
593 The Kuching Formation: A deep marine equivalent of the Sadong Formation, and
594 its implications for the Early Mesozoic tectonic evolution of western and
595 southern Borneo. *Bulletin of the Geological Society of Malaysia*, 76, 101–129.
596 <https://doi.org/10.7186/BGSM76202308>

597 Burton-Johnson, A., Macpherson, C. G., Millar, I. L., Whitehouse, M. J., Ottley, C. J.,
598 & Nowell, G. M. (2020). A Triassic to Jurassic arc in north Borneo:
599 Geochronology, geochemistry, and genesis of the Segama Valley Felsic
600 Intrusions and the Sabah ophiolite. *Gondwana Research*, 84, 229–244.
601 <https://doi.org/10.1016/j.gr.2020.03.006>

602 Burton-Johnson, A., & Cullen, A. B. (2023). Continental rifting in the South China

603 Sea through extension and high heat flow: An extended history. *Gondwana*
604 *Research*, 120, 235–263. <https://doi.org/10.1016/j.gr.2022.07.015>

605 Cao, J., Yang, X., Du, G., & Li, H. (2020). Genesis and tectonic setting of the
606 Malaysian Waterfall granites and tin deposit: Constraints from LA–ICP
607 (MC)–MS zircon U–Pb and cassiterite dating and Sr–Nd–Hf isotopes. *Ore*
608 *Geology Reviews*, 118. <https://doi.org/10.1016/j.oregeorev.2020.103336>

609 Chapman, J. B., Ducea, M. N., Kapp, P., Gehrels, G. E., & DeCelles, P. G. (2017).
610 Spatial and temporal radiogenic isotopic trends of magmatism in Cordilleran
611 orogens. *Gondwana Research*, 48, 189–204.
612 <https://doi.org/10.1016/j.gr.2017.04.019>

613 Cobbing, E.J. (2005), Granites, in Barber, A.J., et al., eds., Sumatra: Geology,
614 Resources and Tectonic Evolution: Geological Society [London] Memoir 31, p.
615 54–62, <https://doi.org/10.1144/gsl.mem.2005.031.01.05>.

616 Corfu, F., Hanchar, J.M., Hoskin, P.W. & Kinny, P. (2003). Atlas of zircon textures.
617 *Reviews in Mineralogy and Geochemistry*, 53 (1), 469–500.
618 <https://doi.org/10.2113/0530469>

619 De Min, A., Velicogna, M., Ziberna, L., Chiaradia, M., Alberti, A., & Marzoli, A.
620 (2020). Triassic magmatism in the European Southern Alps as an early phase of
621 Pangea break-up. *Geological Magazine*, 157(11), 1800–1822.
622 <https://doi.org/10.1017/S0016756820000084>

623 Fan, J.-J., Zhang, B.-C., Zhou, J.-B., Niu, Y., Sun, S.-L., Lv, J.-P., Wang, Y., & Hao,

624 Y.-J. (2024). The Meso-Tethys Ocean: The nature, extension and
 625 spatial-temporal evolution. *Earth-Science Reviews*, 255.
 626 <https://doi.org/10.1016/j.earscirev.2024.104839>

627 Galin, T., Breitfeld, H. T., Hall, R., & Sevastjanova, I. (2017). Provenance of the
 628 Cretaceous–Eocene Rajang Group submarine fan, Sarawak, Malaysia from light
 629 and heavy mineral assemblages and U-Pb zircon geochronology. *Gondwana*
 630 *Research*, 51, 209–233. <https://doi.org/10.1016/j.gr.2017.07.016>

631 Gan, C., Qian, X., Wang, Y., Feng, Q., Zhang, Y., Asis, J. B., & Ao, S. (2022). Late
 632 Cretaceous Granitoids along the Northern Kuching Zone: Implications for the
 633 Paleo-Pacific Subduction in Borneo. *Lithosphere*, 2022(1), 3310613.
 634 <https://doi.org/10.2113/2022/3310613>

635 Gasparon, M., & Varne, R. (1995). Sumatran granitoids and their relationship to
 636 Southeast Asian terranes. *Tectonophysics*, 251(1), 277–299.
 637 [https://doi:10.1016/0040-1951\(95\)00083-6](https://doi:10.1016/0040-1951(95)00083-6).

638 Ghani, A. A., Lo, C.-H., & Chung, S.-L. (2013). Basaltic dykes of the Eastern Belt of
 639 Peninsular Malaysia: The effects of the difference in crustal thickness of
 640 Sibumasu and Indochina. *Journal of Asian Earth Sciences*, 77, 127–139.
 641 <https://doi.org/10.1016/j.jseaes.2013.08.004>

642 Gillespie, M. R., Kendall, R. S., Leslie, A. G., Millar, I. L., Dodd, T. J. H., Kearsey, T.
 643 I., Bide, T. P., Goodenough, K. M., Dobbs, M. R., Lee, M. K. W., & Chiam, K.
 644 (2019). The igneous rocks of Singapore: New insights to Palaeozoic and

645 Mesozoic assembly of the Sukhothai Arc. *Journal of Asian Earth Sciences*, 183,
646 103940. <https://doi.org/10.1016/j.jseaes.2019.103940>

647 Golonka, J. (2007). Late Triassic and Early Jurassic palaeogeography of the world.
648 *Palaeogeography, Palaeoclimatology, Palaeoecology*, 244(1-4), 297-307.
649 <https://doi.org/10.1016/j.palaeo.2006.06.041>

650 Gong, N., Zhang, S-Q., Qi, H., Yuan, G-L., Li, J., Wang, G-H., Liang, X., & Liu, Z-B.
651 (2024). Two stage Mesozoic oceanic subduction and related mantle
652 metasomatism beneath the South Qiangtang terrane with implications for
653 post-collisional magmatism. *Gondwana Research*, 136, 219–235.
654 <https://doi.org/10.1016/j.gr.2024.09.001>.

655 Haile, N.S., McElhinny, M.W., & McDougall, I. (1977). Palaeomagnetic data and
656 radiometric ages from the Cretaceous of West Kalimantan (Borneo), and their
657 significance in interpreting regional structure. *Journal of the Geological Society*.
658 133, 133–144. <https://doi.org/10.1144/gsjgs.133.2.0133>

659 Hall, R. (2012). Late Jurassic–Cenozoic reconstructions of the Indonesian region and
660 the Indian Ocean. *Tectonophysics*, 570-571, 1-41.
661 <https://doi.org/10.1016/j.tecto.2012.04.021>.

662 Hall, R. (2013). Contraction and extension in northern Borneo driven by subduction
663 rollback. *Journal of Asian Earth Sciences*, 76, 399–411.
664 <https://doi.org/10.1016/j.jseaes.2013.04.010>

665 Hall, R., & Breitfeld, T. (2017). Nature and demise of the Proto-South China Sea.

666 *Bulletin of the Geological Society of Malaysia*, 63, 61–76,
667 <https://doi.org/10.7186/bgsm63201703>

668 Hazad, F. I., Ghani, A. A., & Lo, C. H. (2019). Arc related dioritic–granodioritic
669 magmatism from southeastern Peninsular Malaysia and its tectonic implication.
670 *Cretaceous Research*, 95, 208–224. <https://doi.org/10.1016/j.cretres.2018.10.016>

671 Hennig, J., Breitfeld, H. T., Hall, R., & Nugraha, A. M. S. (2017). The Mesozoic
672 tectono-magmatic evolution at the Paleo-Pacific subduction zone in West Borneo.
673 *Gondwana Research*, 48, 292–310. <https://doi.org/10.1016/j.gr.2017.05.001>

674 Hennig-Breitfeld, J., Breitfeld, H. T., Hall, R., BouDagher-Fadel, M., & Thirlwall, M.
675 (2019). A new upper Paleogene to Neogene stratigraphy for Sarawak and Labuan
676 in northwestern Borneo: Paleogeography of the eastern Sundaland margin.
677 *Earth-Science Reviews*, 190, 1–32.
678 <https://doi.org/10.1016/j.earscirev.2018.12.006>

679 Hennig-Breitfeld, J., Breitfeld, H. T., Sang, D. Q., Vinh, M. K., Long, T. V., Thirlwall,
680 M., & Cuong, T. X. (2021). Ages and character of igneous rocks of the Da Lat
681 Zone in SE Vietnam and adjacent offshore regions (Cuu Long and Nam Con Son
682 basins). *Journal of Asian Earth Sciences*, 218.
683 <https://doi.org/10.1016/j.jseaes.2021.104878>

684 Hieu, P.T., Yang, Y.Z., Binh, D.Q., Nguyen, T.B.T., Dung, L.T., & Chen, F. (2015).
685 Late Permian to Early Triassic crustal evolution of the Kontum massif, central
686 Vietnam: Zircon U-Pb ages and geochemical and Nd-Hf isotopic composition of

687 the Hai Van granitoid complex. *International Geology Review*. 57(15), 1877–
688 1888, <https://doi.org/10.1080/00206814.2015.1031194>.

689 Hou, L., Xiong, F., Wang, W., Guo, L., Peng, H., Ni, S., & Zhang, Q. (2019).
690 Carboniferous-Triassic felsic igneous rocks and typical mineral deposits in the
691 Truong Son orogenic belt, SE Asia: Implications for Paleo-Tethyan tectonic
692 evolution and metallogeny. *Ore Geology Reviews*, 112, 103036,
693 <https://doi.org/10.1016/j.oregeorev.2019.103036>

694 Hsu, C. C. (2016), Detrital zircon U-Pb and Hf isotopic study in northwestern
695 Sumatra, Indonesia: Master Thesis, National Taiwan University, p. 1-158.

696 Hu, P.Y., Li, C., Li, J., Wang, M., Xie, C.M., & Wu, Y.W. (2014). Zircon U–Pb–Hf
697 isotopes and whole-rock geochemistry of gneissic granites from the Jitang
698 complex in Leiwuqi area, eastern Tibet, China: record of the closure of the
699 Paleo-Tethys Ocean. *Tectonophysics*, 623, 83–99.
700 <https://doi.org/10.1016/j.tecto.2014.03.018>

701 Hu, Z.C., Liu, Y.S., Gao, S., Liu, W., Yang, L., Zhang, W., Tong, X., Lin, L., Zong,
702 K.Q., Li, M., Chen, H. & Zhou, L. (2012). Improved in situ Hf isotope ratio
703 analysis of zircon using newly designed X skimmer cone and Jet sample cone in
704 combination with the addition of nitrogen by laser ablation multiple collector
705 ICP-MS. *Journal of Analytical Atomic Spectrometry*, 27, 1391–1399.
706 <https://doi.org/10.1039/C2JA30078H>

707 Hutchison, C.S. (1996). The ‘Rajang Accretionary Prism’ and ‘Lupar Line’ problem

708 of Borneo. In: Hall, R., Blundell, D.J. (Eds.), Tectonic Evolution of SE Asia.
 709 *Geological Society of London Special Publication*. Vol. 106, pp. 247–261.
 710 Hutchison, C.S. (2005). Geology of North-West Borneo: Sarawak, Brunei and Sabah:
 711 Amsterdam, The Netherlands, Elsevier, 421 p.
 712 Ishiga, H. & Ishiyama, D. (1987). Jurassic accretionary complex in Kaminokuni
 713 Terrane, southwestern Hokkaido, Japan. *Mining Geology*, 37, 381–394.
 714 Isozaki, Y., Aoki, K., Nakama, T., & Yanai, S. (2010). New insight into a
 715 subduction-related orogen: A reappraisal of the geotectonic framework and
 716 evolution of the Japanese Islands. *Gondwana Research*, 18(1), 82–105.
 717 <https://doi.org/10.1016/j.gr.2010.02.015>
 718 Jamil, A., Ghani, A. A., Zaw, K., Osman, S., & Quek, L. X. (2016). Origin and
 719 tectonic implications of the ~200 Ma, collision-related Jerai pluton of the
 720 Western Granite Belt, Peninsular Malaysia. *Journal of Asian Earth Sciences*, 127,
 721 32–46. <https://doi.org/10.1016/j.jseaes.2016.06.004>
 722 Li, L.-S., Capitanio, F. A., Cawood, P. A., Wu, B.-J., Zhai, M.-G., & Wang, X.-L.
 723 (2024). Double subduction controls on long-lived continental tectonics and
 724 subcontinental mantle temperatures. *Geology*, 52(11), 836–840.
 725 <https://doi.org/10.1130/g52232.1>
 726 Li, J., Sha, J., McLoughlin, S., & Wang, X. (2019). Mesozoic and Cenozoic
 727 palaeogeography, palaeoclimate and palaeoecology in the eastern Tethys.
 728 *Palaeogeography, Palaeoclimatology, Palaeoecology*, 515, 1–5.

729 <https://doi.org/10.1016/j.palaeo.2018.11.014>

730 Li, S., Chung, S.-L., Lai, Y.-M., Ghani, A. A., Lee, H.-Y., & Murtadha, S. (2020).
731 Mesozoic juvenile crustal formation in the easternmost Tethys: Zircon Hf
732 isotopic evidence from Sumatran granitoids, Indonesia. *Geology*, 48(10), 1002–
733 1005. <https://doi.org/10.1130/g47304.1>

734 Li, Z. X., & Li, X. H. (2007). Formation of the 1300-km-wide intracontinental orogen
735 and postorogenic magmatic province in Mesozoic South China: A flat-slab
736 subduction model. *Geology*, 35(2), 179–182. <https://doi.org/10.1130/g23193a.1>

737 Liew, T.C., & Page, R.W. (1985). U-Pb zircon dating of granitoid plutons from the
738 West Coast Province of Peninsular Malaysia. *Journal of the Geological Society*,
739 142 (3): 515–526, <https://doi.org/10.1144/gsjgs.142.3.0515>

740 Liu, Y.S., Gao, S., Hu, Z.C., Gao, C.G., Zong, K.Q. & Wang, D.B. (2010).
741 Continental and oceanic crust recycling-induced melt-peridotite interactions in
742 the Trans-North China Orogen: U-Pb dating, Hf isotopes and trace elements in
743 zircons of mantle xenoliths. *Journal of Petrology*, 51(1 – 2): 537 – 571.
744 <https://doi.org/10.1093/petrology/egp082>

745 Liu, L., Hu, R.-Z., Zhong, H., Yang, J.-H., Kang, L.-F., Zhang, X.-C., Fu, Y.-Z., Mao,
746 W., & Tang, Y.-W. (2020). Petrogenesis of multistage S-type granites from the
747 Malay Peninsula in the Southeast Asian tin belt and their relationship to Tethyan
748 evolution. *Gondwana Research*, 84, 20–37.
749 <https://doi.org/10.1016/j.gr.2020.02.013>

750 Lyu, T., Zhu, Z., & Wu, B. (2019). Subducting slab morphology and mantle transition

751 zone upwelling in double-slab subduction models with inward-dipping directions.

752 *Geophysical Journal International*, 218(3), 2089–2105.

753 <https://doi.org/10.1093/gji/ggz268>

754 Mange, M.A., & Maurer, H.F.W. (1992). Heavy Minerals in Colour. Chapman & Hall,

755 London. <https://doi.org/10.1007/978-94-011-2308-2>.

756 Martinez, F., & Taylor, B. (2002). Mantle wedge control on back-arc crustal accretion.

757 *Nature*, 416(6879), 417–420. <https://doi:10.1038/416417a>.

758 Metcalfe, I. (1996). Pre-Cretaceous evolution of SE Asian terrane, in Hall, R., and

759 Blundell, D., eds., Tectonic Evolution of Southeast Asia: Geological Society

760 [London] Special Publication, 106: 97–122,

761 <https://doi.org/10.1144/GSL.SP.1996.106.01.09>

762 Metcalfe, I., 2009. Late Palaeozoic and Mesozoic tectonic and palaeogeographical

763 evolution of SE Asia. In: Buffetaut, E., Cuny, G., Le Loeuff, J., Suteethorn, V.

764 (Eds.), Late Palaeozoic and Mesozoic Ecosystems in SE Asia Geological Society

765 of London Special Publication. 315, pp. 7–23.

766 Metcalfe, I. (2011). Palaeozoic–Mesozoic history of SE Asia. In R. Hall, M. A.

767 Cottam, & M. E. J. Wilson (Eds.), *The SE Asian Gateway: History and Tectonics*

768 *of the Australia-Asia Collision*. Geological Society of London.

769 <https://doi.org/10.1144/sp355.2>

770 Metcalfe, I. (2013). Gondwana dispersion and Asian accretion: Tectonic and

771 palaeogeographic evolution of eastern Tethys. *Journal of Asian Earth Sciences*,

772 66, 1-33. <https://doi.org/10.1016/j.jseas.2012.12.020>

773 Metcalfe, I. (2017). Tectonic evolution of Sundaland. *Bulletin of the Geological*

774 *Society of Malaysia*, 63, 2760.

775 Metcalfe, I. (2021). Multiple Tethyan ocean basins and orogenic belts in Asia.

776 *Gondwana Research*, 100, 87-130. <https://doi.org/10.1016/j.gr.2021.01.012>.

777 Minh, N.T., Dung, N.T., Hung, D.D., Minh, P., Yu, Y., & Hieu, P.T. (2020). Zircon

778 U-Pb ages, geochemistry and isotopic characteristics of the Chu Lai granitic

779 pluton in the Kontum massif, central Vietnam. *Mineralogy and Petrology*, 114(4),

780 289–303, <https://doi.org/10.1007/s00710-020-00707-x>

781 Morley, C. K. (2018). Understanding Sibumasu in the context of ribbon continents.

782 *Gondwana Research*, 64, 184–215. <https://doi.org/10.1016/j.gr.2018.07.006>

783 Müller, R. D., Seton, M., Zahirovic, S., Williams, S. E., Matthews, K. J., Wright, N.

784 M., Shephard, G. E., Maloney, K. T., Barnett-Moore, N., Hosseinpour, M.,

785 Bower, D. J., & Cannon, J. (2016). Ocean Basin Evolution and Global-Scale

786 Plate Reorganization Events Since Pangea Breakup. *Annual Review of Earth and*

787 *Planetary Sciences*, 44(1), 107–138.

788 <https://doi.org/10.1146/annurev-earth-060115-012211>

789 Müller, R. D., Zahirovic, S., Williams, S. E., Cannon, J., Seton, M., Bower, D. J.,

790 Tetley, M. G., Heine, C., Le Breton, E., Liu, S., Russell, S. H. J., Yang, T.,

791 Leonard, J., & Gurnis, M. (2019). A Global Plate Model Including Lithospheric

792 Deformation Along Major Rifts and Orogens Since the Triassic. *Tectonics*, 38(6),

1884–1907. <https://doi.org/10.1029/2018tc005462>

Nance, R.D., Murphy, J.B., & Santosh, M., (2014). The supercontinent cycle: A retrospective essay. *Gondwana Research*, 25, 4–29, <https://doi.org/10.1016/j.gr.2012.12.026>

Ng, S. W.-P., Whitehouse, M. J., Searle, M. P., Robb, L. J., Ghani, A. A., Chung, S.-L., Oliver, G. J. H., Sone, M., Gardiner, N. J., & Roselee, M. H. (2015). Petrogenesis of Malaysian granitoids in the Southeast Asian tin belt: Part 2. U-Pb zircon geochronology and tectonic model. *Geological Society of America Bulletin*, 127(9-10), 1238–1258. <https://doi.org/10.1130/b31214.1>

Ng, S. W.-P., Whitehouse, M. J., Roselee, M. H., Teschner, C., Murtadha, S., Oliver, G. J. H., Ghani, A. A., & Chang, S.-C. (2017). Late Triassic granites from Bangka, Indonesia: A continuation of the Main Range granite province of the South-East Asian Tin Belt. *Journal of Asian Earth Sciences*, 138, 548–561. <https://doi.org/10.1016/j.jseaes.2017.03.002>

Nguyen, H.H. (2019). The Cenozoic evolution of the South Vietnam margin of the South China Sea and the origin of coastal placer deposits [Ph.D. thesis]: London, University of London, 177 p.

Oliver, G., Zaw, K., Hotson, M., Meffre, S., & Manka, T. (2014). U–Pb zircon geochronology of Early Permian to Late Triassic rocks from Singapore and Johor: A plate tectonic reinterpretation. *Gondwana Research*, 26(1), 132–143. <https://doi.org/10.1016/j.gr.2013.03.019>

814 Olsen, P. E. (1997). Stratigraphic record of the early Mesozoic breakup of Pangea in
815 the Laurasia-Gondwana rift system. *Annual Review of Earth and Planetary*
816 *Sciences*, 25(1), 337-401. <https://doi.org/10.1146/annurev.earth.25.1.337>

817 Pastor-Galán, D., Spencer, C. J., Furukawa, T., & Tsujimori, T. (2021). Evidence for
818 crustal removal, tectonic erosion and flare-ups from the Japanese evolving
819 forearc sediment provenance. *Earth and Planetary Science Letters*, 564, 116893.
820 <https://doi.org/10.1016/j.epsl.2021.116893>

821 Pearce, N.J.G., Perkins, W.T., Westgate, J.A., Gorton, M.P., Jackson, S.E., Neal, C.R.,
822 & Chenery, S.P. (1997). A compilation of new and published major and trace
823 element data for NIST SRM 610 and NIST SRM 612 Glass Reference Materials.
824 *Geostandards Newsletter*. 21, 115–144.
825 <https://doi.org/10.1111/j.1751-908X.1997.tb00538.x>.

826 Pieters, P. E., Surono, & Noya, Y. (1993). Geology of the Putussibau Sheet area,
827 Kalimantan. Geological Survey of Indonesia, Directorate of Mineral Resources,
828 Geological Research and Development Centre, Bandung, Quadrangle 1616,
829 1:250000.

830 Qian, X., Yu, Y., Wang, Y., Gan, C., Zhang, Y., Asis, J. B., & Ao, S. (2022). Late
831 Cretaceous Nature of SW Borneo and Paleo-Pacific Subduction: New Insights
832 from the Granitoids in the Schwaner Mountains. *Lithosphere*, 2022(1), 8483732.
833 <https://doi.org/10.2113/2022/8483732>

834 Qian, X., Bai, T., Yu, Y., Mustapha, K. A., Sheldrick, T. C., Gan, C., & Wang, Y.

835 (2023). Multiple stages of continental rifting in Eastern Peninsular Malaysia:
 836 new insights from Jurassic–Cretaceous granitoids. *Journal of the Geological*
 837 *Society*, 180(5), jgs2023-025. <https://doi.org/10.1144/jgs2023-025>
 838 Qiu, L., Kong, R., Yan, D.-P., Mu, H.-X., Sun, W., Sun, S., Han, Y., Li, C., Zhang, L.,
 839 Cao, F., & Ariser, S. (2022a). Paleo–Pacific plate subduction on the eastern Asian
 840 margin: Insights from the Jurassic foreland system of the overriding plate.
 841 *Geological Society of America Bulletin*, 134(9-10), 2305–2320.
 842 <https://doi.org/10.1130/b36118.1>
 843 Qiu, L., Li, X., Li, X., Yan, D.-P., Ren, M., Zhang, L., & Cheng, G. (2022b).
 844 Petrogenesis of early cretaceous intermediate to felsic rocks in Shanghai, South
 845 China: Magmatic response to Paleo-Pacific plate subduction. *Tectonophysics*,
 846 838, 229469. <https://doi.org/10.1016/j.tecto.2022.229469>
 847 Quek, L., Lai, Y.-M., Ghani, A. A., Roselee, M. H., Lee, H.-Y., Iizuka, Y., Umor, M.
 848 R., Pecha, M., Lin, Y.-L., Rahmat, R., & Jamil, A. (2021a). Peninsular Malaysia
 849 transitional geodynamic process from Gondwana to Pangaea: New constraints
 850 from 500 to 200 Ma magmatic zircon U-Pb ages and Hf isotopic compositions.
 851 *Gondwana Research*, 94, 56–72. <https://doi.org/10.1016/j.gr.2021.03.001>
 852 Quek, L. X., Lee, T.-Y., Ghani, A. A., Lai, Y.-M., Roselee, M. H., Lee, H.-Y., Iizuka,
 853 Y., Lin, Y.-L., Yeh, M.-W., Amran, M. A., & Rahmat, R. (2021b). Tracing detrital
 854 signature from Indochina in Peninsular Malaysia fluvial sediment: Possible
 855 detrital zircon recycling into West Borneo Cenozoic sediments. *Journal of Asian*

856 *Earth Sciences*, 218, 104876. <https://doi.org/10.1016/j.jseaes.2021.104876>

857 Quek, L. X., Li, S., Morley, C. K., Ghani, A. A., Zhu, J., Roselee, M. H., Murthadha,
858 S., Rahmat, R., Lai, Y.-M., & Lintjewas, L. (2023). Southwest Borneo, an
859 autochthonous Pangea-Eurasia assembly proxy: Insights from detrital zircon
860 record. *Geology*. 51, 785–790. <https://doi.org/10.1130/g50966.1>

861 Searle, M. P., Whitehouse, M. J., Robb, L. J., Ghani, A. A., Hutchison, C. S., Sone, M.,
862 Ng, S. W. P., Roselee, M. H., Chung, S. L., & Oliver, G. J. H. (2012). Tectonic
863 evolution of the Sibumasu–Indochina terrane collision zone in Thailand and
864 Malaysia: constraints from new U–Pb zircon chronology of SE Asian tin
865 granitoids. *Journal of the Geological Society*, 169(4), 489–500.
866 <https://doi.org/10.1144/0016-76492011-107>

867 Setiawan, N.I., Osanai, Y., Nakano, N., Adachi, T., Setiadji, L.D., & Wahyudiono, J.
868 (2013). Late Triassic metatonalite from the Schwaner Mountains in West
869 Kalimantan and its contribution to sedimentary provenance in the Sundaland.
870 *Berita Sedimentologi*, 12, 4–12.

871 Shellnutt, J.G., Lan, C.Y., Van Long, T., Usuki, T., Yang, H.J., Mertzman, S.A., Iizuka,
872 Y., Chung, S.L., Wang, K.L., & Hsu, W.Y. (2013). Formation of Cretaceous
873 Cordilleran and post-orogenic granites and their microgranular enclaves from the
874 Dalat zone, southern Vietnam: Tectonic implications for the evolution of
875 Southeast Asia. *Lithos.* 182–183, 229–241,
876 <https://doi.org/10.1016/j.lithos.2013.09.016>

877 Shi, M.F., Lin, F.C., Fan, W.Y., Deng, Q., Cong, F., Tran, M.D., Zhu, H.P., & Wang, H.
878 (2015). Zircon U–Pb ages and geochemistry of granitoids in the Truong Son
879 terrane, Vietnam: Tectonic and metallogenic implications. *Journal of Asian Earth*
880 *Sciences*, 101, 101–120. <https://doi.org/10.1016/j.jseaes.2015.02.001>.

881 Sun, B., Kaus, B. J. P., Yang, J., Lu, G., Wang, X., Wang, K., & Zhao, L. (2021).
882 Subduction Polarity Reversal Triggered by Oceanic Plateau Accretion:
883 Implications for Induced Subduction Initiation. *Geophysical Research Letters*,
884 e2021GL095299. <https://doi.org/10.1029/2021gl095299>

885 Sundell, K. E., & Macdonald, F. A. (2022). The tectonic context of hafnium isotopes
886 in zircon. *Earth and Planetary Science Letters*, 584.
887 <https://doi.org/10.1016/j.epsl.2022.117426>

888 Tran, H.T., Zaw, K., Halpin, J.A., Manaka, T., Meffre, S., Lai, C.K., Lee, Y., Le, H.V.,
889 & Dinh, S. (2014), The Tam Ky-Phuoc Son Shear Zone in central Vietnam:
890 Tectonic and metallogenic implications. *Gondwana Research*, 26, 144–164,
891 <https://doi.org/10.1016/j.gr.2013.04.008>.

892 van Hattum, M. W. A., Hall, R., Pickard, A. L., & Nichols, G. J. (2006). Southeast
893 Asian sediments not from Asia: Provenance and geochronology of north Borneo
894 sandstones. *Geology*, 34(7), 589–592. <https://doi.org/10.1130/g21939.1>

895 van Hattum, M. W. A., Hall, R., Pickard, A. L., & Nichols, G. J. (2013). Provenance
896 and geochronology of Cenozoic sandstones of northern Borneo. *Journal of Asian*
897 *Earth Sciences*, 76, 266–282. <https://doi.org/10.1016/j.jseaes.2013.02.033>

898 Vermeesch, P., Resentini, A., & Garzanti, E. (2016). An R package for statistical
 899 provenance analysis. *Sedimentary Geology*. 336, 14–25. [https://doi.org/10.1016/j.](https://doi.org/10.1016/j.sedgeo.2016.01.009)
 900 [sedgeo.2016.01.009](https://doi.org/10.1016/j.sedgeo.2016.01.009).

901 Wang, C., Mitchell, R. N., Murphy, J. B., Peng, P., & Spencer, C. J. (2020). The role
 902 of megacontinents in the supercontinent cycle. *Geology*, 49(4), 402-406.
 903 <https://doi.org/10.1130/g47988.1>.

904 Wang, S., Mo, Y., Wang, C., & Ye, P. (2016). Paleotethyan evolution of the Indochina
 905 Block as deduced from granites in northern Laos. *Gondwana Research*, 38, 183–
 906 196. <https://doi.org/10.1016/j.gr.2015.11.011>.

907 Wang, Y., Qian, X., Zhang, Y., Gan, C., Zhang, A., Zhang, F., Feng, Q., Cawood, P. A.,
 908 & Zhang, P. (2021a). Southern extension of the Paleotethyan zone in SE Asia:
 909 Evidence from the Permo-Triassic granitoids in Malaysia and West Indonesia.
 910 *Lithos*, 398–399. <https://doi.org/10.1016/j.lithos.2021.106336>

911 Wang, Y., Zhang, A., Qian, X., Asis, J. B., Feng, Q., Gan, C., Zhang, Y., Cawood, P.
 912 A., Wang, W., & Zhang, P. (2021b). Cretaceous Kuching accretionary orogenesis
 913 in Malaysia Sarawak: Geochronological and geochemical constraints from mafic
 914 and sedimentary rocks. *Lithos*, 400-401.
 915 <https://doi.org/10.1016/j.lithos.2021.106425>

916 Wang, Y., Liu, Z., Murtadha, S., Cawood, P. A., Qian, X., Ghani, A., Gan, C., Zhang,
 917 Y., Wang, Y., Li, S., & Zhang, P. (2022a). Jurassic subduction of the
 918 Paleo-Pacific plate in Southeast Asia: New insights from the igneous and

919 sedimentary rocks in West Borneo. *Journal of Asian Earth Sciences*, 232, 105111.
920 <https://doi.org/10.1016/j.jseaes.2022.105111>

921 Wang, Y., Wu, S., Qian, X., Cawood, P. A., Lu, X., Gan, C., Asis, J. B., & Zhang, P.
922 (2022b). Early Cretaceous subduction in NW Kalimantan: Geochronological and
923 geochemical constraints from the Raya and Mensibau igneous rocks. *Gondwana*
924 *Research*, 101, 243–256. <https://doi.org/10.1016/j.gr.2021.08.006>

925 Wang, Y., Qian, X., Bin Asis, J., Cawood, P. A., Wu, S., Zhang, Y., Feng, Q., & Lu, X.
926 (2023). “Where, when and why” for the arc-trench gap from Mesozoic
927 Paleo-Pacific subduction zone: Sabah Triassic-Cretaceous igneous records in
928 East Borneo. *Gondwana Research*, 117, 117–138.
929 <https://doi.org/10.1016/j.gr.2023.01.008>

930 Wang, Y., Qian, X., Cawood, P. A., Gan, C., Zhang, Y., Zhang, F., Asis, J. B., Yan, Y.,
931 & Wang, C. (2024). Temporal-spatial patterns of Mesozoic Paleo-Pacific and
932 Tethyan supra-subduction systems in SE Asia: Key observations and
933 controversies in Borneo and its surroundings. *Earth-Science Reviews*, 252,
934 104762. <https://doi.org/10.1016/j.earscirev.2024.104762>

935 Wiedenbeck, M., Allé, P., Corfu, F., Griffin, W.L., Meier, M., Oberli, F., Quadt, A.V.,
936 Roddick, J.C., & Spiegel, W. (1995). Three natural zircon standards for U-Th-Pb,
937 Lu-Hf, trace element and REE analyses. *Geostandards Newsletter*. 19, 1–23.
938 <https://doi.org/10.1111/j.1751-908X.1995.tb00147.x>

939 Williams, P.R., Johnston, C.R., Almond, R.A., & Simamora, W.H. (1988). Late

940 Cretaceous to Early Tertiary structural elements of West Kalimantan.
 941 *Tectonophysics*, 148, 279–297. [https://doi.org/10.1016/0040-1951\(88\)90135-7](https://doi.org/10.1016/0040-1951(88)90135-7)

942 Wu, F. Y., Yang, J. H., Xu, Y. G., Wilde, S. A., & Richard, J. W. (2019). Destruction of
 943 the North China Craton in the Mesozoic. *Annual Review of Earth and Planetary*
 944 *Sciences*, 47(1), 173–195. <https://doi.org/10.1146/annurev-earth-053018-060342>

945 Yu, Y., Qian, X., Azlan Mustapha, K., Sheldrick, T. C., Gan, C., Zhang, Y., & Wang, Y.
 946 (2022). Late Paleozoic–Early Mesozoic granitic rocks in Eastern Peninsular
 947 Malaysia: New insights for the subduction and evolution of the Paleo-Tethys.
 948 *Journal of Asian Earth Sciences*, 239, 105427.
 949 <https://doi.org/10.1016/j.jseaes.2022.105427>

950 Zhang, K., Liao, J., & Gerya, T. (2024). Onset of double subduction controls plate
 951 motion reorganisation. *Nature Communications*, 15(1), 1513.
 952 <https://doi.org/10.1038/s41467-024-44764-8>

953 Zhang, W., Hu, Z., & Spectroscopy, A. (2020). Estimation of Isotopic Reference
 954 Values for Pure Materials and Geological Reference Materials. *Atomic*
 955 *Spectroscopy*, 2020, 41(3):93–102. <https://doi.org/10.46770/AS.2020.03.001>

956 Zhang, X., Chung, S.-L., Lai, Y.-M., Ghani, A. A., Murtadha, S., Lee, H.-Y., & Hsu,
 957 C.-C. (2019). A 6000-km-long Neo-Tethyan arc system with coherent magmatic
 958 flare-ups and lulls in South Asia. *Geology*, 47(6), 573–576.
 959 <https://doi.org/10.1130/g46172.1>

960 Zhang, Z.-Y., Hou, Z.-Q., Lü, Q.-T., Zhang, X.-W., Pan, X.-F., Fan, X.-K., Zhang,

Y.-Q., Wang, C.-G., & Lü, Y.-J. (2023). Crustal architectural controls on critical metal ore systems in South China based on Hf isotopic mapping. *Geology*, 51(8), 738-742. <https://doi.org/10.1130/g51203.1>

Zhao, Q. (2025). AGU Tectonics Supporting Information for: Interaction between the Tethyan and Paleo-Pacific tectonic domains in Southeast Asia: Late Triassic initiation of an inward-dipping double subduction system [Dataset]. *Mendeley Data*, V1. <https://doi.org/10.17632/8g669bt2bt.1>

Zhu, K. Y., Li, Z. X., Xu, X. S., & Wilde, S. A. (2013). Late triassic melting of a thickened crust in southeastern China: Evidence for flat-slab subduction of the Paleo-Pacific plate. *Journal of Asian Earth Sciences*, 74, 265 – 279. <https://doi.org/10.1016/j.jseaes.2013.01.010>

Zhu, R. X., & Xu, Y. G. (2019). The subduction of the West Pacific Plate and the destruction of the North China Craton. *Science China Earth Sciences*, 62(9), 1340–1350. <https://doi.org/10.1007/s11430-018-9356-y>

Zhou, Y., Carter, A., Wu, J., Yao, Y., Zhu, R., Liu, H., Liu, W., Zhao, Q., Zhu, Z., Yan, Y., & Liu, Q. (2023). Nature of the Paleo-Pacific Subduction Along the East Asian Continental Margin in the Mesozoic: Insights From the Sedimentary Record of West Sarawak, Borneo. *Geophysical Research Letters*, 50(8). <https://doi.org/10.1029/2022gl102370>

Figure 1.

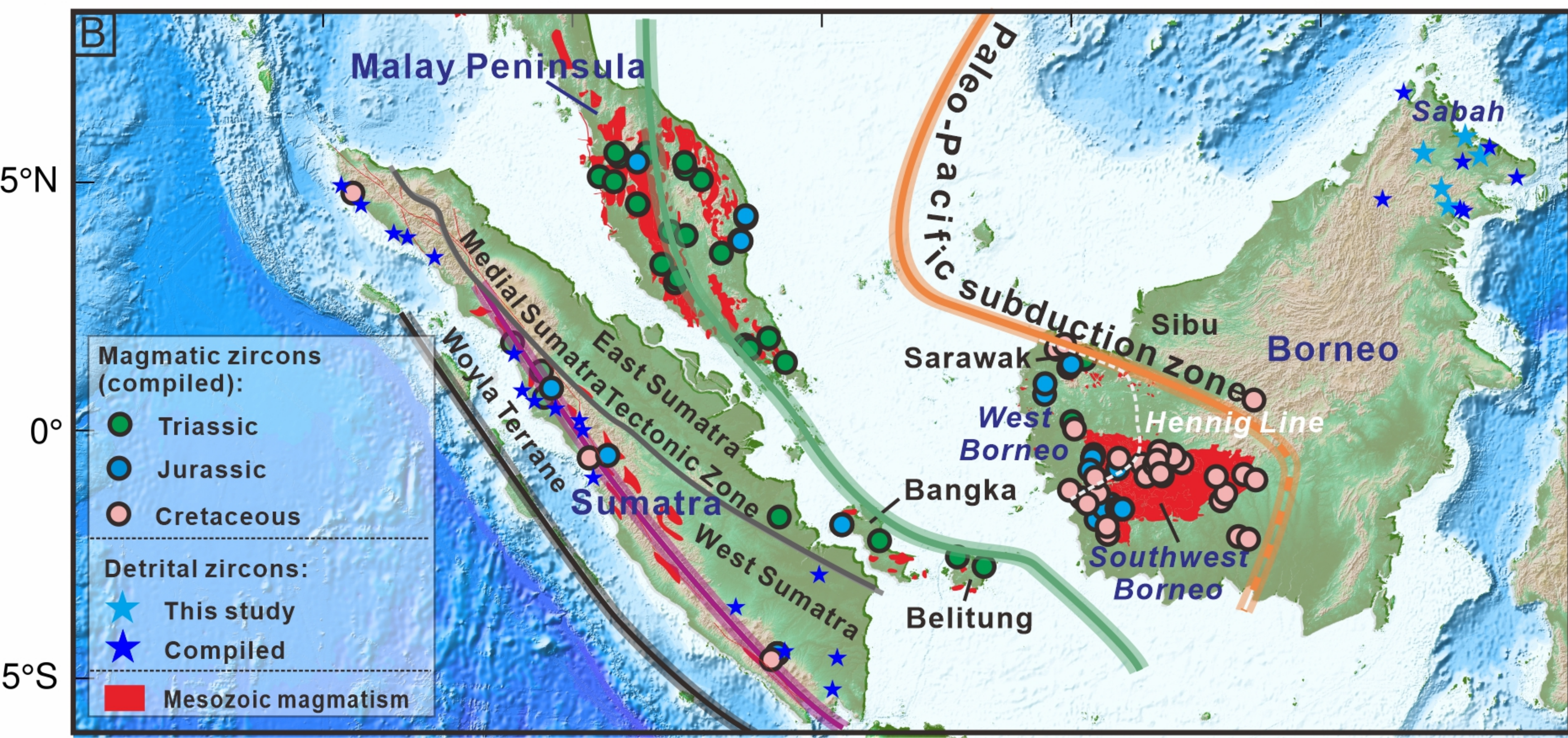
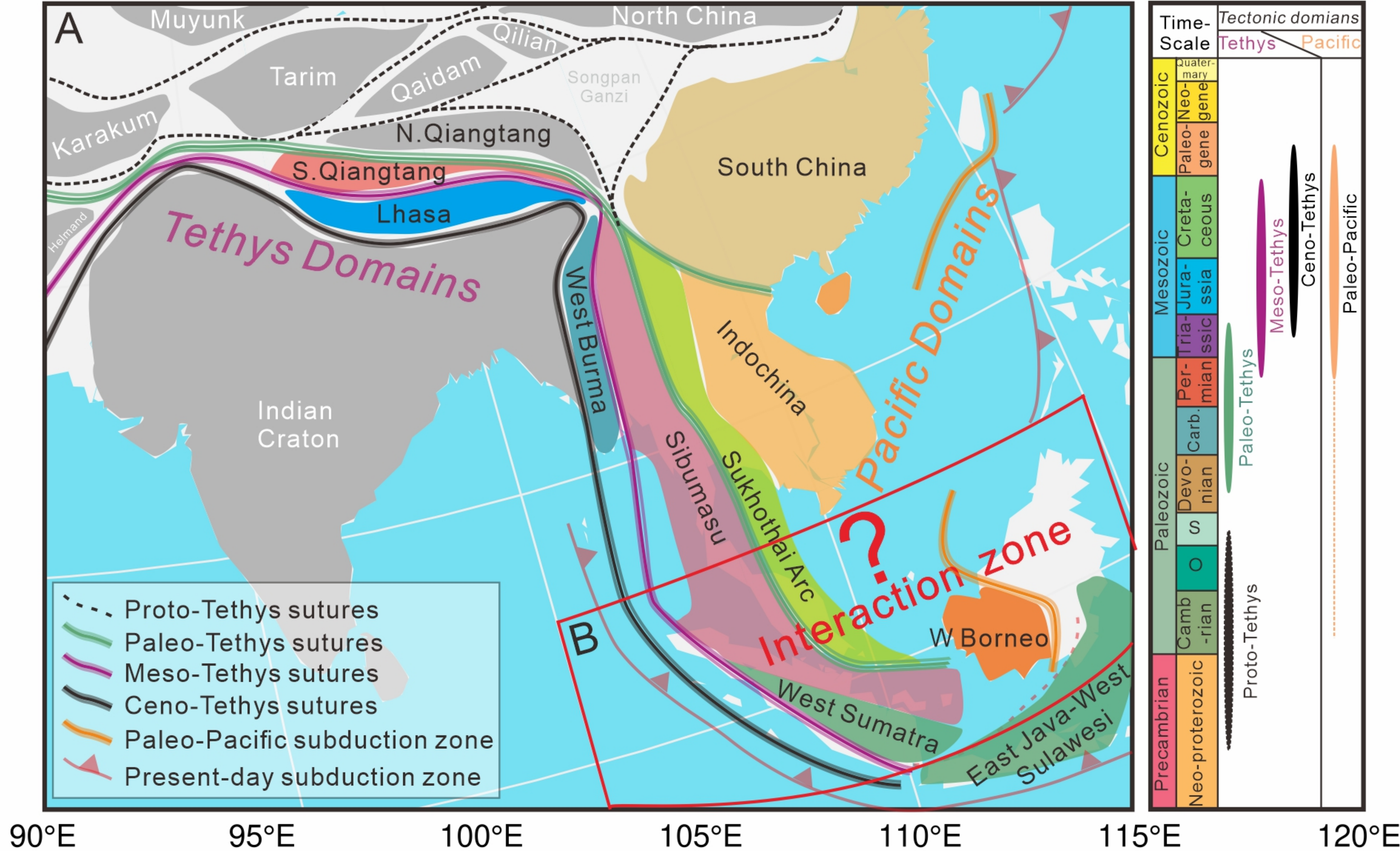
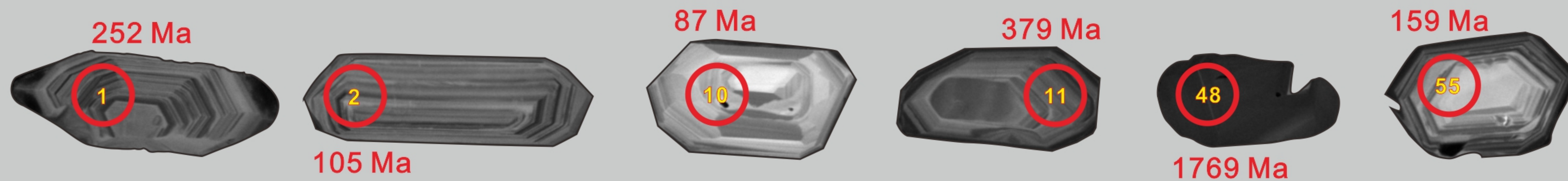


Figure 2.

K-03

100 μm



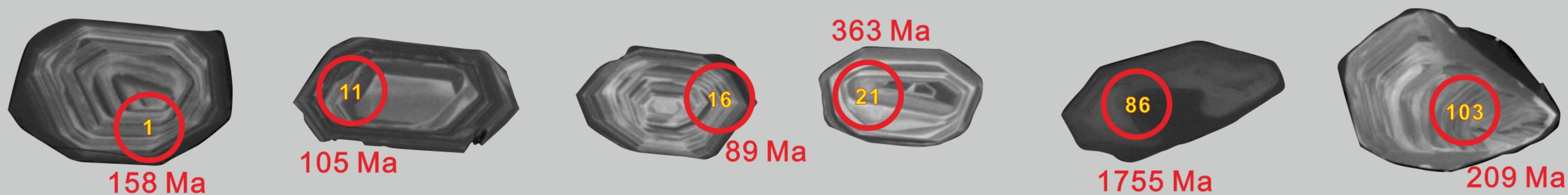
K-01

100 μm



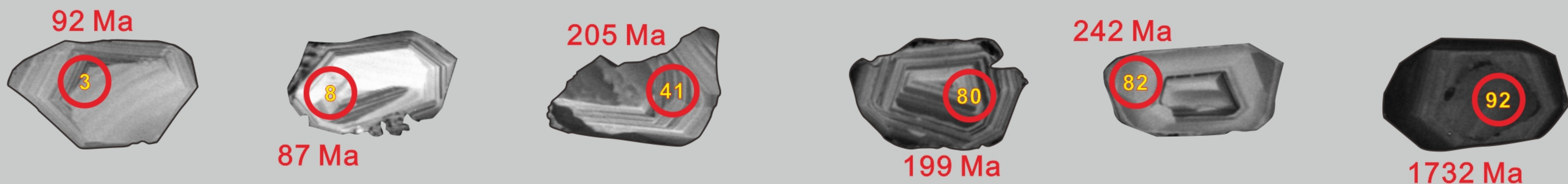
SK-02

100 μm



SK-06

100 μm



TB-10B

100 μm

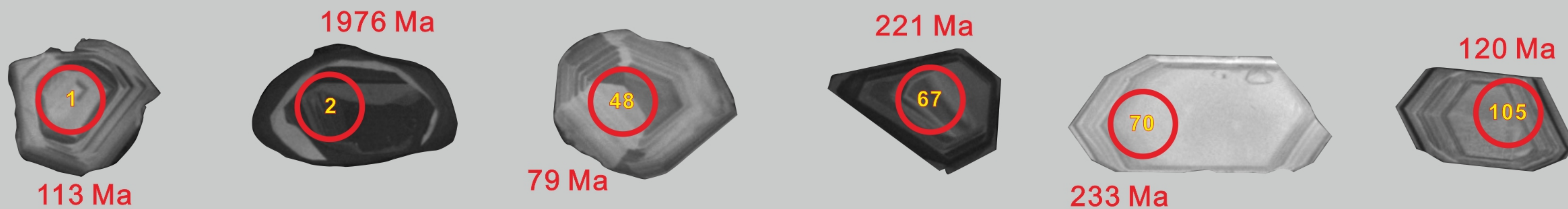


Figure 3.

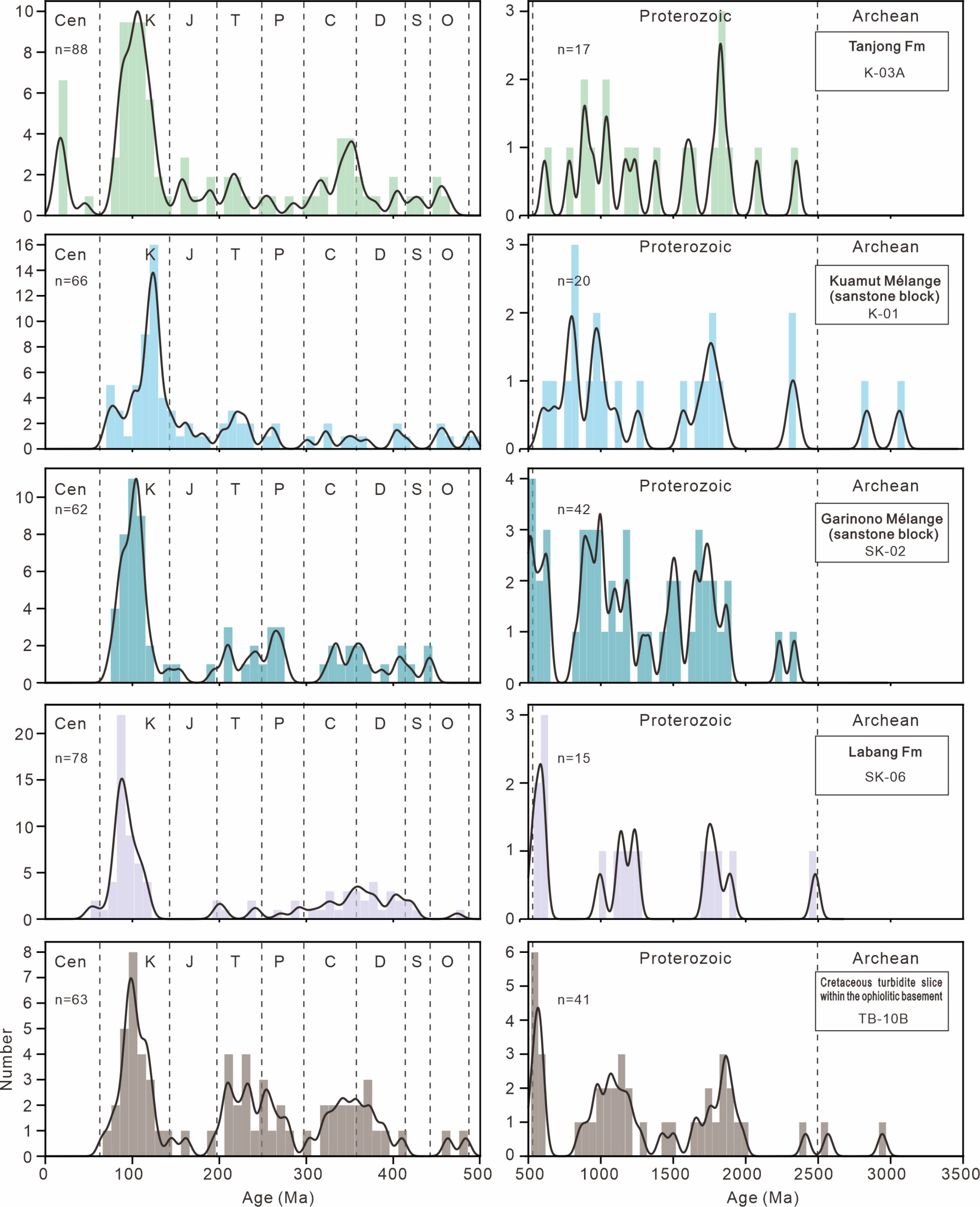


Figure 4.

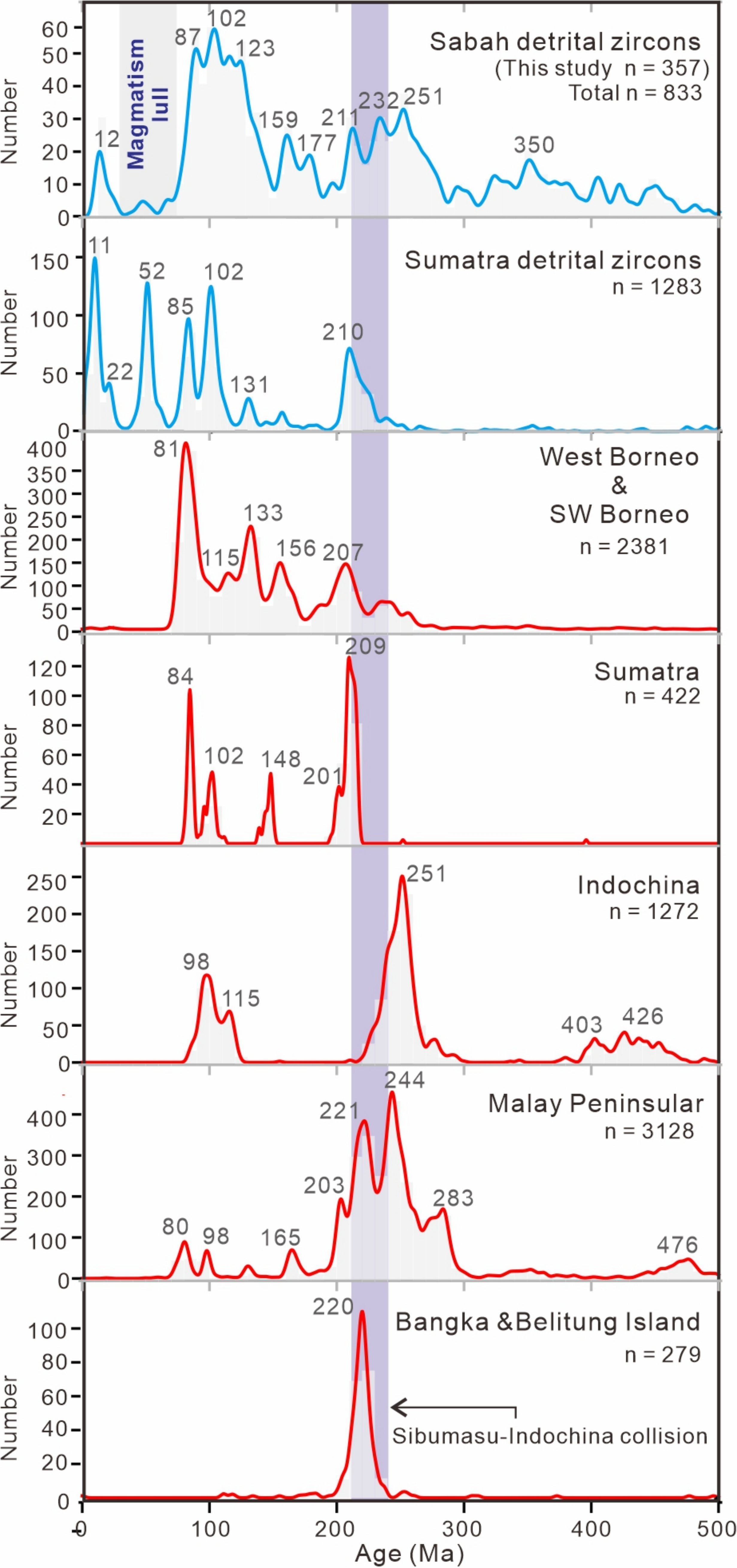


Figure 5.

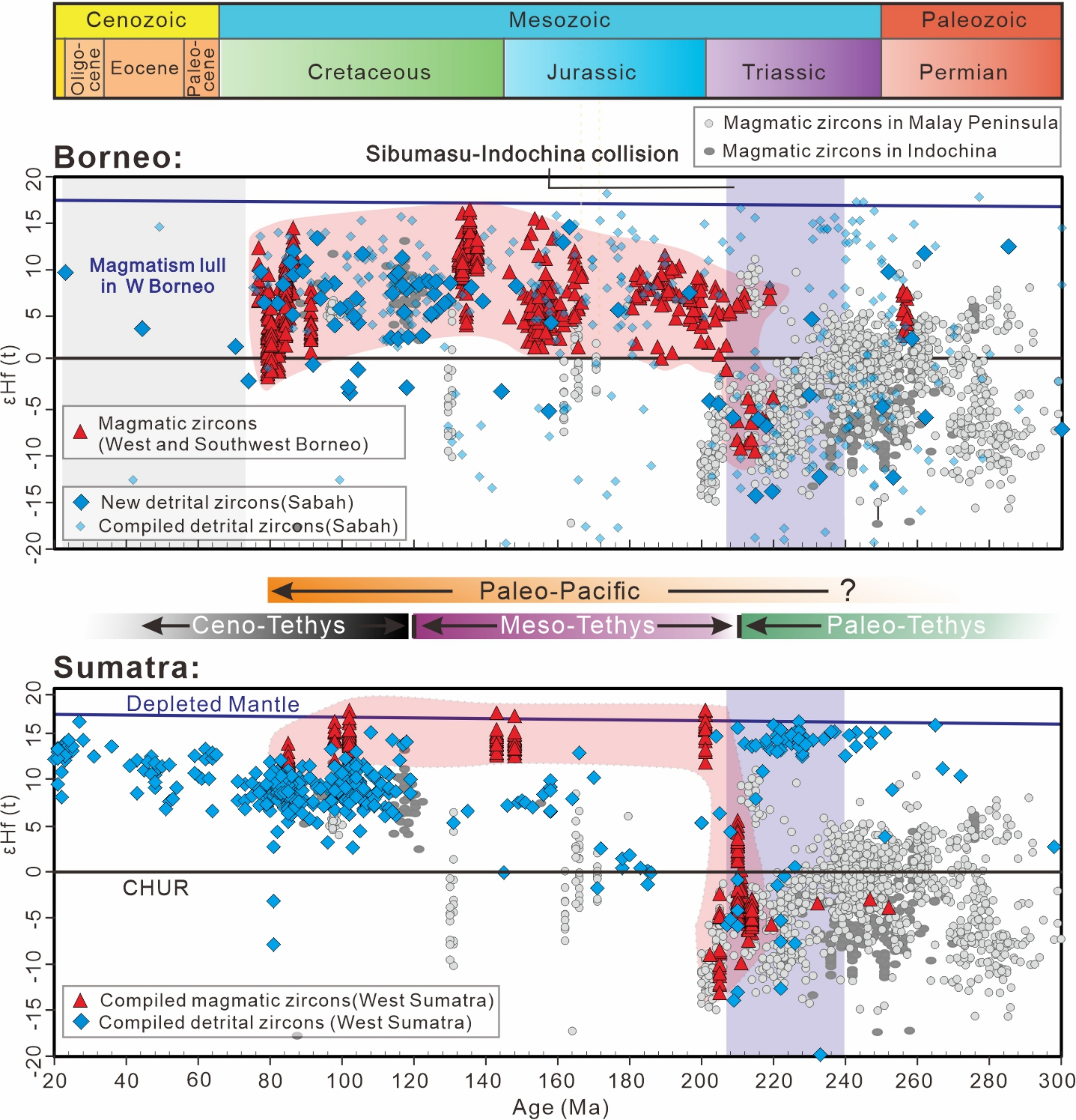


Figure 6.

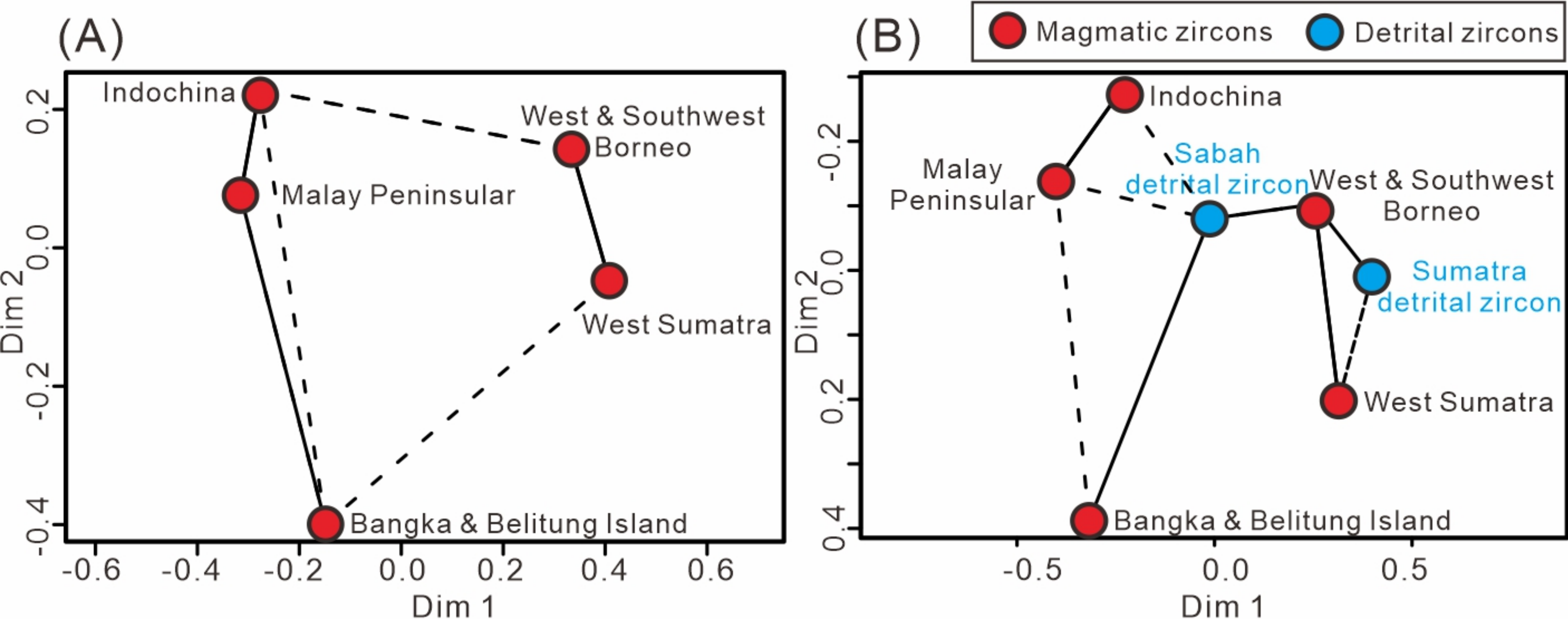


Figure 7.

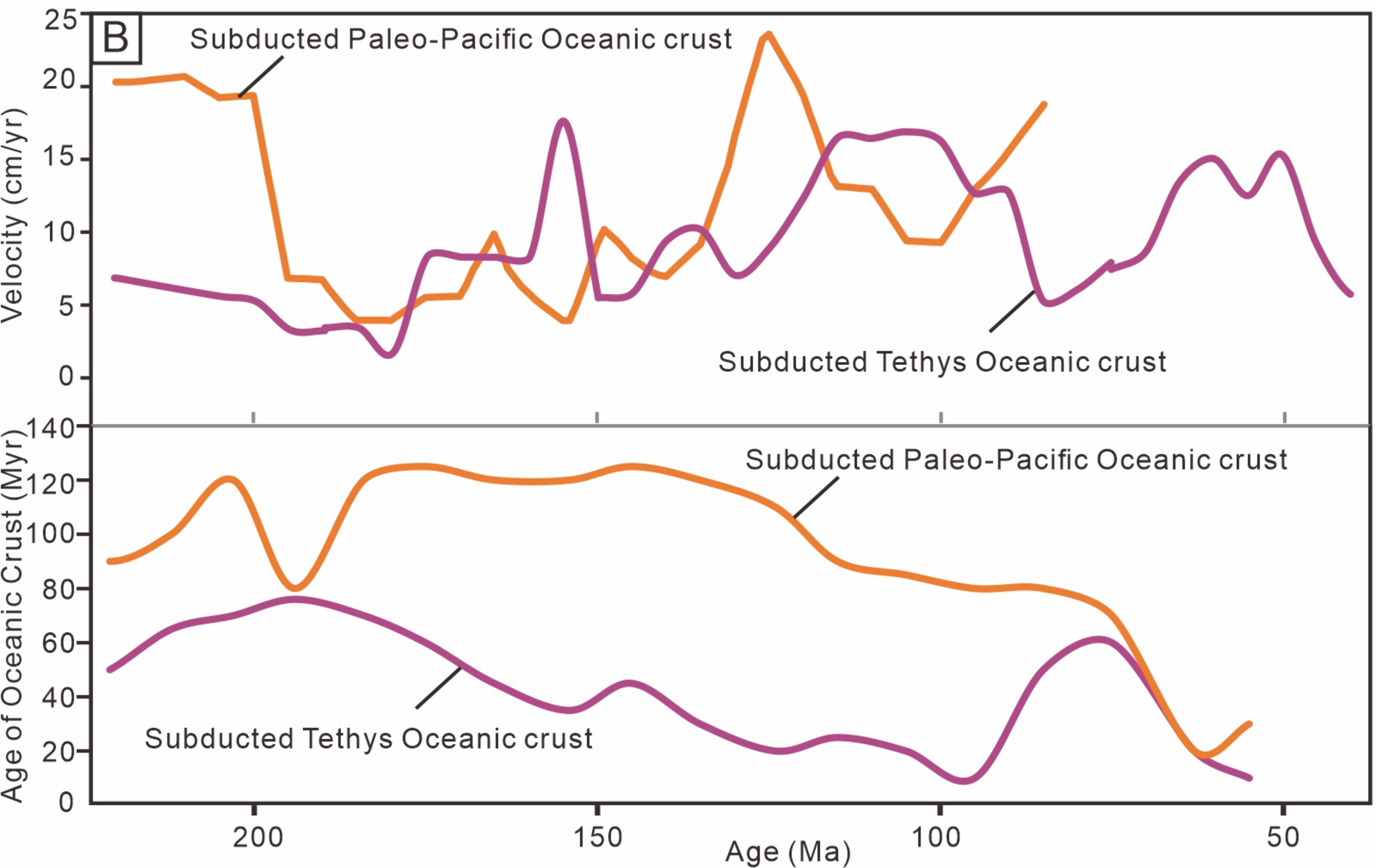
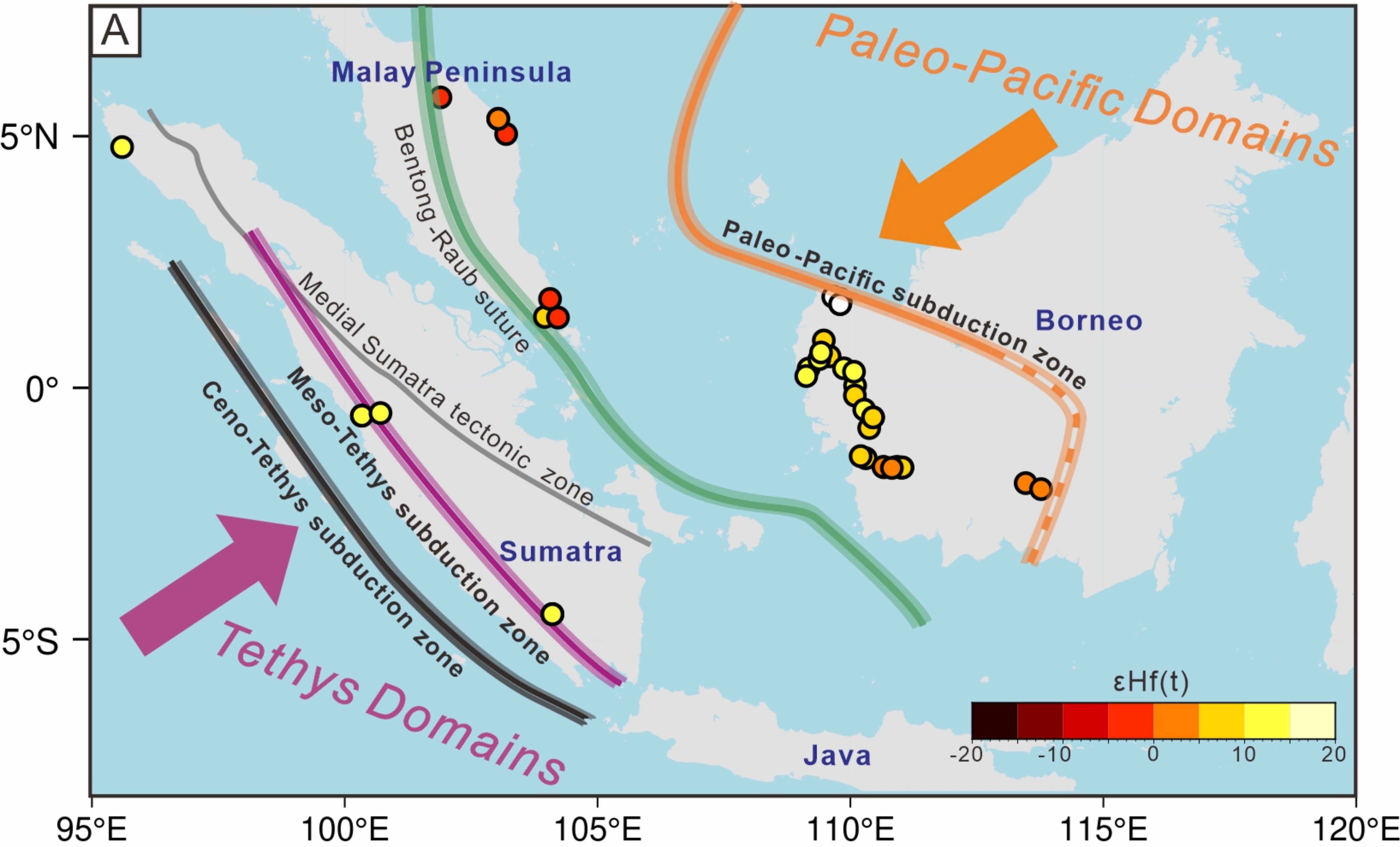


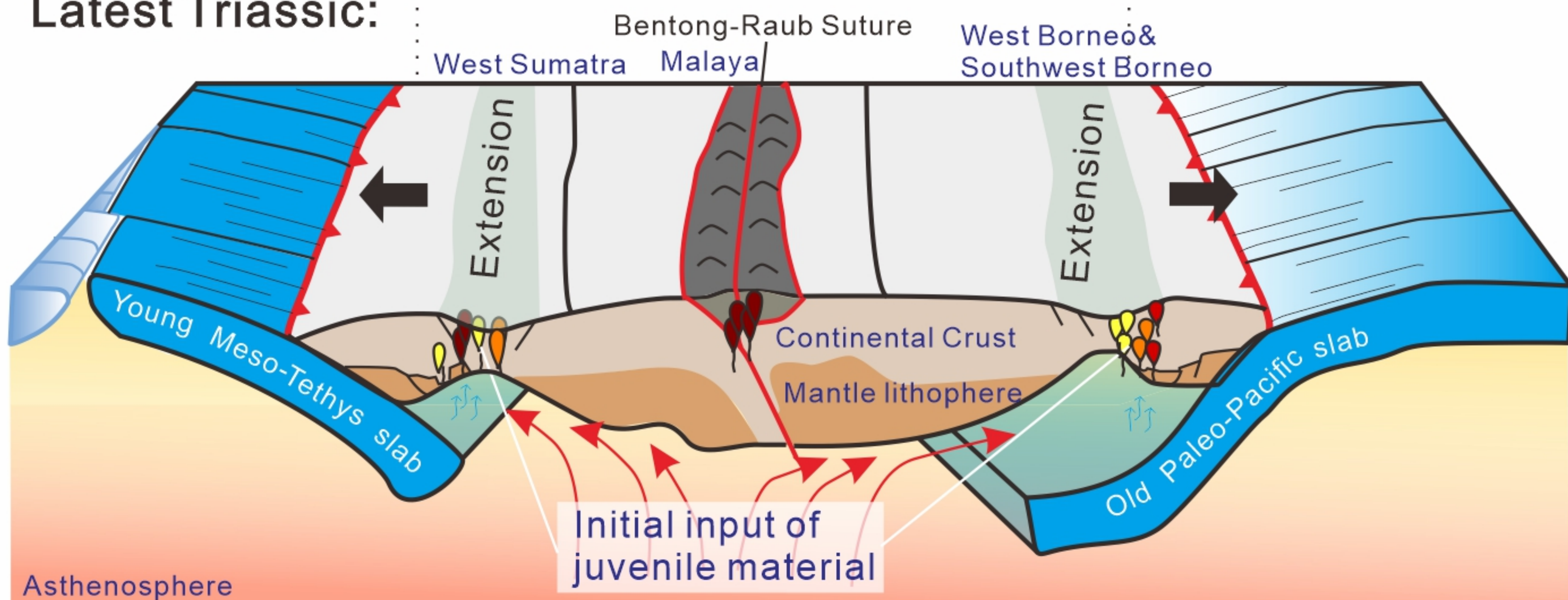
Figure 8.

Tethys Domain

Interaction Zone

Paleo-Pacific Domain

Latest Triassic:



Jurassic-Cretaceous:

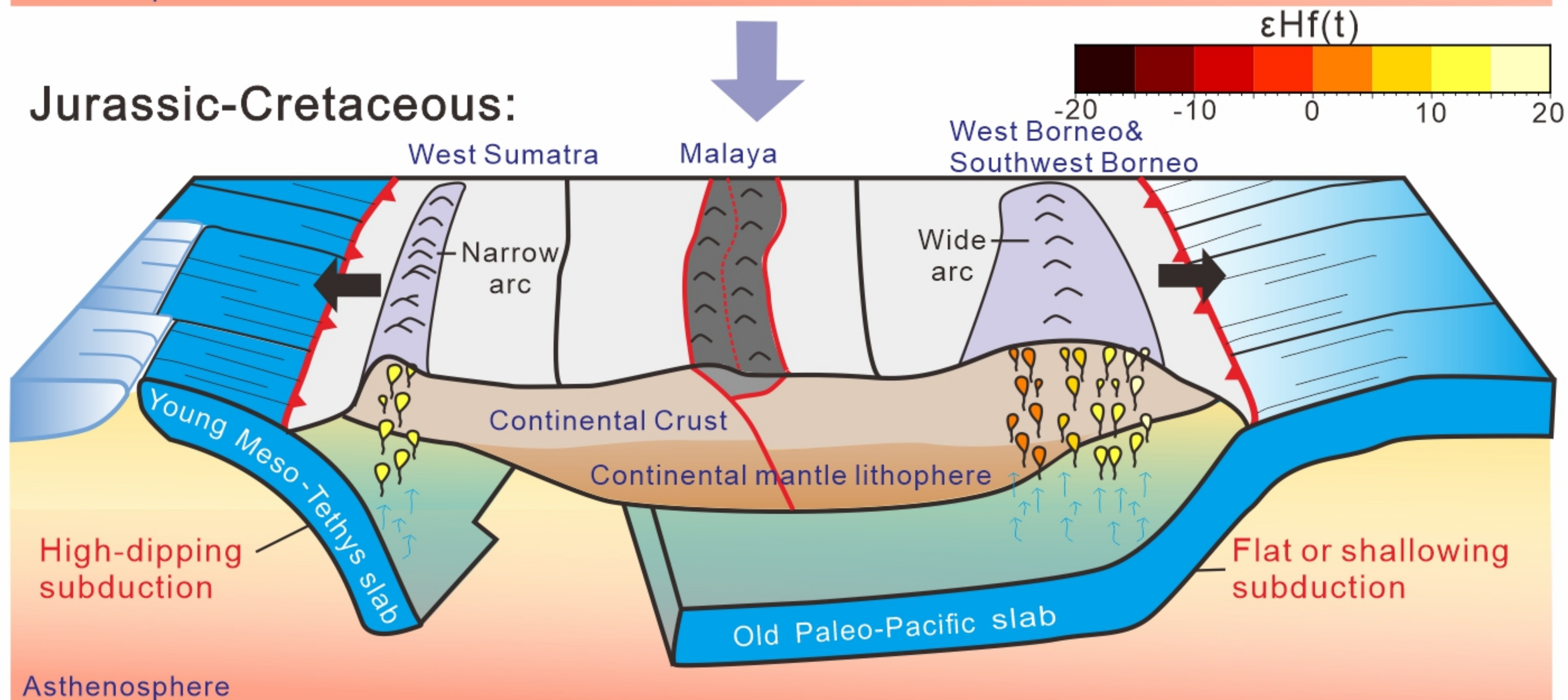
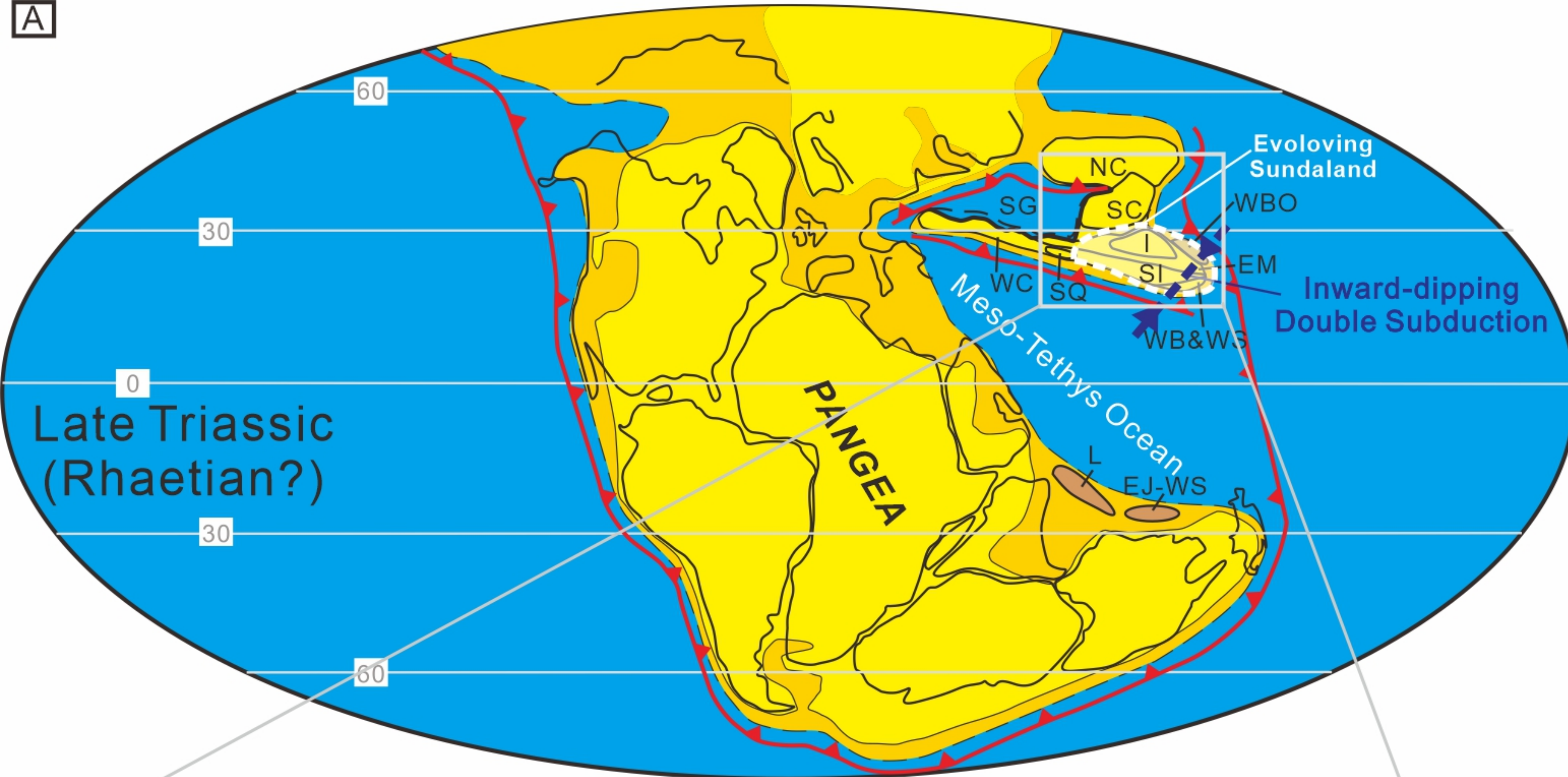


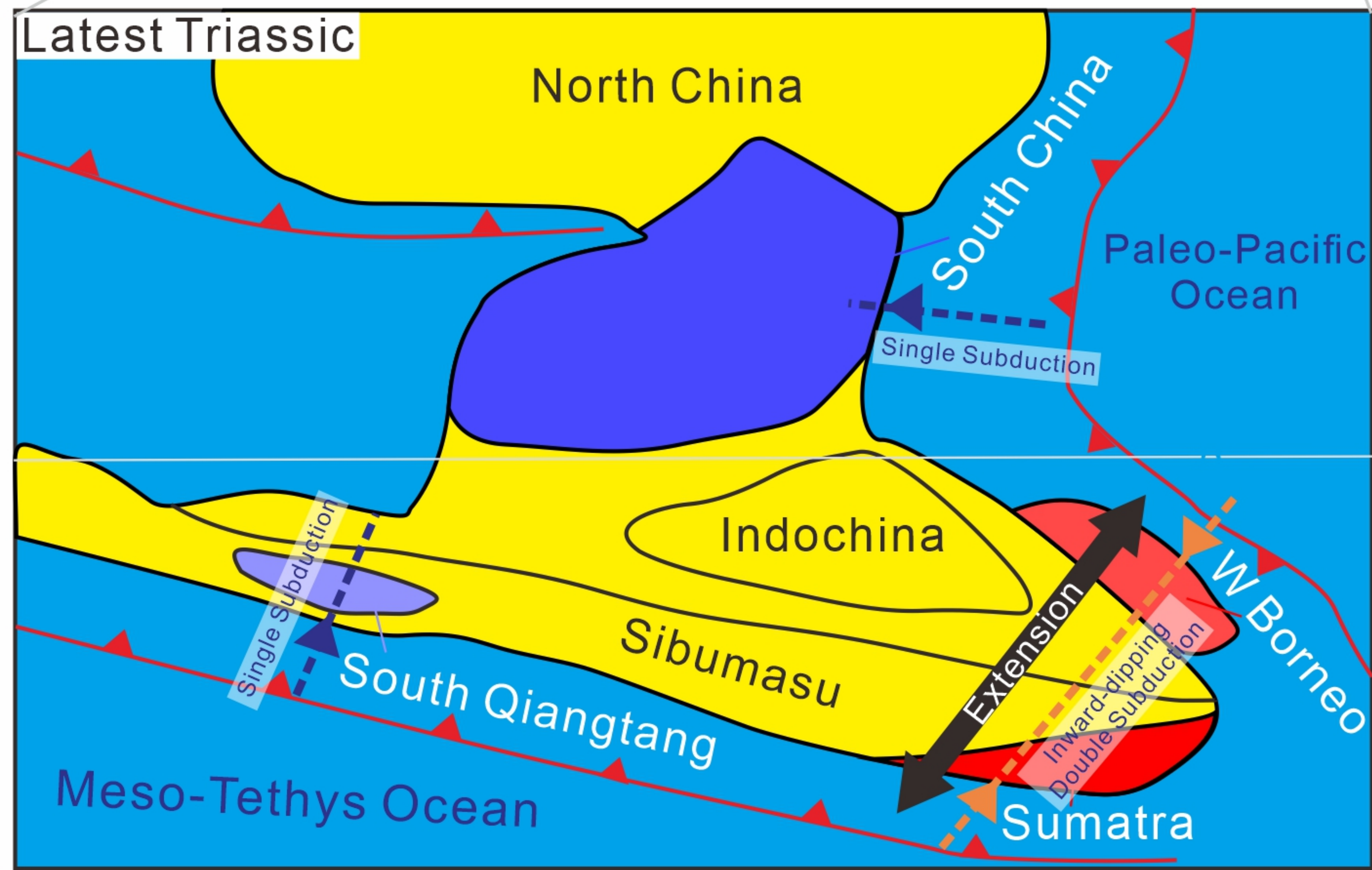
Figure 9.

A



- NC: North China
- SC: South China
- SG: Songpan Ganzi accretionary complex
- I: Indochina
- SI: Simao
- WBO: West Borneo
- EM: East Malaya
- WB&WS: West Buma and West Sumatra
- WC: Western Cimmerian Continent
- L: Lhasa
- EJ-WS: East Java-West Sulawesi

Latest Triassic



B

